ATMOSPHERIC ENVIRONMENT: X 29 (2026) 100430

Contents lists available at ScienceDirect

Atmospheric Environment: X

journal homepage: www.journals.elsevier.com/atmospheric-environment-x

Potential effects of climate change on global air quality and human health

Racha Samermit [a,*], Thanapat Jansakoo [b], Shinichiro Fujimori [a,c,d], Saritha Sudharmma Vishwanathan [a,e]

[a] Department of Environmental Engineering, Kyoto University, C1-3, Kyotodaigaku Katsura, Nishikyo-ku, Kyoto, Japan
[b] Department of Environment for Sustainability, Faculty of Environment, Kasetsart University, Thailand
[c] National Institute for Environmental Studies (NIES), Tsukuba, Ibaraki, Japan
[d] International Institute for Applied System Analysis (IIASA), Laxenburg, Austria
[e] Public Systems Group, Indian Institute of Management Ahmedabad, Gujarat, India

ARTICLE INFO

Keywords:
Climate change
GCAP2.0
GEOS-Chem
Global air quality
Health impact
Ozone
$PM_{2.5}$

ABSTRACT

Climate change alters air quality and associated health outcomes. Climate-driven meteorological variables such as temperature, precipitation, and relative humidity influence transport, chemical transformation, and removal of air pollutants, particularly fine particulate matter ($PM_{2.5}$) and ozone (O_3). Here, we investigated the impacts of climate change on global $PM_{2.5}$ and O_3 concentrations via one-way coupling of an atmospheric chemical transport model (CTM) with the outputs of a general circulation model. We examined the impact on future air quality under three climate scenarios: SSP1–2.6, SSP2–4.5, and SSP5–8.5 of the Scenario Model Intercomparison Project (ScenarioMIP) for the mid-century (2040–2049) and the end of the century (2090–2099). To isolate the effect of climate change, anthropogenic and natural emissions were fixed at 2015 levels, enabling quantification of meteorologically driven changes in air quality and mortality. Our results show that climate forcing can trigger substantial regional variations in pollutant levels, with the global mean $PM_{2.5}$ concentration changing by −0.01 μg m^{-3} to −0.57 μg m^{-3} and the O_3 level from −0.05 ppbv to −1.20 ppbv. In our experimental framework–where primary and precursor emissions as well as chemical boundary conditions are held constant at 2015 levels–surface $PM_{2.5}$ and O_3 concentrations generally decline under future climate conditions due to meteorological shifts. These changes reflect the isolated effects of climate-driven meteorology rather than the combined climate-emission pathways associated with SSP-RCP scenarios. Although mean global pollutant changes appear to be modest, the associated health benefits are not negligible, corresponding to more than 0.2 million deaths avoided from $PM_{2.5}$ exposure, and 0.08 million deaths from O_3 exposure, when aggregated across all scenarios. Our results underscore the importance of considering climate–meteorology interactions when assessing future air quality and its public-health impacts.

1. Introduction

Climate change is a major global challenge, with widespread possible impacts on ecosystems, economies, and human health. One key pathway through which climate change threatens health is by worsening air quality, raising exposure to harmful pollutants such as fine particulate matter ($PM_{2.5}$) and ground-level ozone (O_3) (Kinney, 2008; WHO, 2021). The World Health Organization (WHO) has reported that poor ambient air quality was associated with an estimated 4.2 million premature deaths in 2019 (WHO, https://www.who.int/health-topics/air-pollution#tab=tab_2). Long-term exposure to $PM_{2.5}$ is associated with elevated risks such as ischemic heart disease, stroke, chronic obstructive pulmonary disease (COPD), lung cancer, and lower respiratory infections, making it one of the largest environmental contributors to global mortality (Burnett et al., 2014; Miller et al., 2007; Pope and Dockery, 2006; Pope III et al., 2002). In addition, long-term O_3 exposure is primarily linked to respiratory impacts, including reduced lung function, airway inflammation, and exacerbation of asthma (Dimakopoulou et al., 2020; Jerrett et al., 2009). Both pollutants pose substantial health risks, particularly for sensitive populations, especially elderly, children, and individuals with pre-existing cardiovascular or respiratory diseases (EPA, 2013; WHO, 2021).

Climate change and air pollution are closely linked. An Intergovernmental Panel on Climate Change (IPCC) report indicated that rising

* Corresponding author.
E-mail address: samermit.racha.86e@st.kyoto-u.ac.jp (R. Samermit).

https://doi.org/10.1016/j.aeaoa.2026.100430
Received 21 October 2025; Received in revised form 2 February 2026; Accepted 19 February 2026
Available online 20 February 2026

temperatures, altered precipitation patterns, and more extreme weather events are directly linked to changes in air-pollution levels. Climate change significantly influences local air quality by modifying meteorological conditions (Andersson and Langner, 2007; Im et al., 2023; Westervelt et al., 2016; Zhai et al., 2019). For example, climate-driven temperature increases attributable to rising carbon dioxide (CO_2) concentrations can elevate surface O_3 levels (Schnell et al., 2016). Changes in precipitation affect $PM_{2.5}$ concentrations by influencing wet deposition processes that affect pollutant removal (Tai et al., 2010). Climate change increases the frequency and intensity of wildfires, which are associated with high levels of $PM_{2.5}$ precursor emission (Fang et al., 2013; Kinney, 2008). Air pollutants, specifically atmospheric aerosols and short-lived climate forcers (SLCFs), also influence climate by affecting radiative forcing and cloud microphysics, in turn modulating temperature and precipitation patterns (IPCC, 2023; Turnock et al., 2023).

An analysis of how $PM_{2.5}$ and O_3 affect air quality requires consideration of both the emissions and the meteorological conditions that drive pollutant formation and changes in pollutant levels (Von Schneidemesser et al., 2015). Anthropogenic and natural sources of $PM_{2.5}$ and O_3 precursors include methane (CH_4), ammonia (NH_3), nitrogen oxides (NOx), volatile organic compounds (VOCs), and sulfur dioxide (SO_2). All are chemically produced in the atmosphere, leading to the formation of $PM_{2.5}$ and O_3 (Seinfeld and Pandis, 2016). Meteorology greatly affects the transport, dispersion, chemical transformation, and removal of $PM_{2.5}$ and O_3. For example, high temperatures, low humidity, and low wind levels enhance O_3 formation (Koo et al., 2012). $PM_{2.5}$ levels also strongly depend on atmospheric temperature, precipitation, and wind speed (Feng et al., 2012; Hua et al., 2016). Therefore, $PM_{2.5}$ and O_3 concentrations would be expected to vary with climate change (Tai et al., 2010, 2012b; Wang et al., 2023), which is currently rapid. It is also essential to study future mortality associated with air-quality changes attributable to climate variation (Silva et al., 2017; West et al., 2013).

Several studies have examined the effects of climate change on air quality. Many used statistical approaches to project future air quality based on historical relationships between air pollution and meteorological variables (Shen et al., 2017; Tai et al., 2012b; Zhai et al., 2019). However, it has often been assumed that historical pollutant and meteorology relationships will remain valid under changing climate regimes. Other modeling approaches that include chemistry–climate models (CCMs) have been used to simulate climate–chemistry interactions (e.g., Westervelt et al., 2016), but high computational costs often limit the chemical complexity that can be considered. Chemical transport models (CTMs) driven by the offline meteorological fields of general circulation models (GCMs) are more flexible. One-way coupling allows consideration of many detailed chemical scenarios and simplifies analyses of meteorological effects on air quality (e.g., Murray et al., 2021, 2024; Wu et al., 2008).

Climate-driven changes in surface O_3 have been extensively documented across regions (e.g.,Zanis et al., 2022), while numerous studies have also examined the influence of meteorology and climate variability on $PM_{2.5}$ (e.g., Hua et al., 2016; Krishnaveni et al., 2024; Lin et al., 2024; Tai et al., 2012a; 2010; Turnock et al., 2020; Westervelt et al., 2016; Zhai et al., 2019). Compared to O_3, $PM_{2.5}$ responses tend to be more spatially variable and uncertain due to their shorter atmospheric lifetime and stronger dependence on local conditions (Turnock et al., 2020). Building on the CTM-based framework of Murray et al. (2021), we investigated how the use of future meteorological data that reflect climate change influences global air-quality. We performed CTM simulations using future meteorological fields derived from compatible outputs of the Phase 6 Climate Model Intercomparison Project (CMIP6).

Previous studies (Dawson et al., 2007; Doherty et al., 2013; Westervelt et al., 2016) generally found that the effects of climate change on $PM_{2.5}$ and O_3 concentrations were small or spatially inconsistent across regions; we acknowledge those conclusions. However, we further hypothesized that climate-driven meteorological changes, particularly in terms of temperature, precipitation, wind speed, and relative humidity, could in fact notably impact global and regional air quality, in turn exacerbating health risks in vulnerable regions, underscoring the need to consider how climate change might affect future health.

This study therefore explored whether future climate-driven meteorological conditions should be explicitly incorporated into global air-quality assessments. We quantified the effects of $PM_{2.5}$ and O_3 concentrations on health. To this end, we employed the GEOS-Chem model driven by the meteorology of Global Change and Air Pollution version 2.0 (GCAP 2.0). In this study, we isolated the impacts of climate-driven meteorological changes by keeping anthropogenic and natural emissions, and chemical boundary conditions constant at 2015 levels. Therefore, the simulated changes in $PM_{2.5}$ and O_3 reflected meteorology-only sensitivity responses rather than projections of future air quality under the SSP-RCP emission pathways. The atmospheric composition changes associated with evolving emissions–particularly modifications in precursor emissions, methane, dust, and biogenic sources–are not represented. Consequently, the results should be interpreted as the isolated influence of climate-driven meteorology, not as the full air-quality outcomes expected under future socioeconomic scenarios characterized fixed at present-day conditions. This enabled clear attribution of the air-quality responses to climate change. In summary, this study investigated how climate change influences global $PM_{2.5}$ and O_3 air quality. We determined how climate-driven meteorological changes alone may affect future pollutant concentrations at different warming levels. We further evaluated the associated health implications, highlighting that climate impacts alone could significantly shape future global and regional air-quality risks. These findings are particularly relevant in terms of future air-quality projections, underscoring the importance of considering climate change when estimating pollutant levels and associated health risks.

2. Methodology

We used a Goddard Earth Observing System-Chemistry model (GEOS-Chem) driven by GCAP2.0 meteorology to simulate the future spatial distributions of global air quality. We examined changes in the surface $PM_{2.5}$ and O_3 concentrations driven solely by the future climate changes of the SSP1–2.6, SSP2–4.5 and SSP5–8.5 scenarios. During all simulations, anthropogenic and natural emissions were held constant at 2015 levels. Methane concentrations were prescribed using the default background methane mixing ratio in GEOS-Chem, with methane emissions excluded. Specifically, the surface anthropogenic emissions follow the harmonized year of CMIP6-compliant CEDS inventory (version 2017-05-18; Hoesly et al., 2018). The emission processing follows the GCAP2.0 framework described by Murray et al. (2021). We conducted three main assessments. First, we compared the $PM_{2.5}$ and O_3 concentrations under each climate scenario to those simulated by present-day meteorology. Second, we derived correlations between changes in $PM_{2.5}$ and O_3 levels and variations in the dominant meteorological factors. Lastly, we assessed changes in mortality attributable to $PM_{2.5}$ and O_3 exposure, to evaluate the potential health implications of climate-driven air-quality changes. The overall research framework is illustrated in Fig. 1.

2.1. GEOS-chem driven by GCAP2.0 meteorology

This study used GEOS-Chem, a global three-dimensional atmospheric chemical transport model (v.14-1-1) (Bey et al., 2001; http://www.geos-chem.org) driven by the GCAP2.0 meteorological fields of Murray et al. (2021). Generally, the model simulates HO_x-NO_x-VOC-O_3-BrO_x-aerosol tropospheric chemistry using updated soil NO_x emissions (Keller et al., 2014; Mao et al., 2013; Parrella et al., 2012). We performed GEOS-Chem simulation at the native 4° x 5° resolution with 40 vertical layers. The evaluation of Jansakoo et al. (2024b) has shown that using this resolution does not substantially affect the regional scale

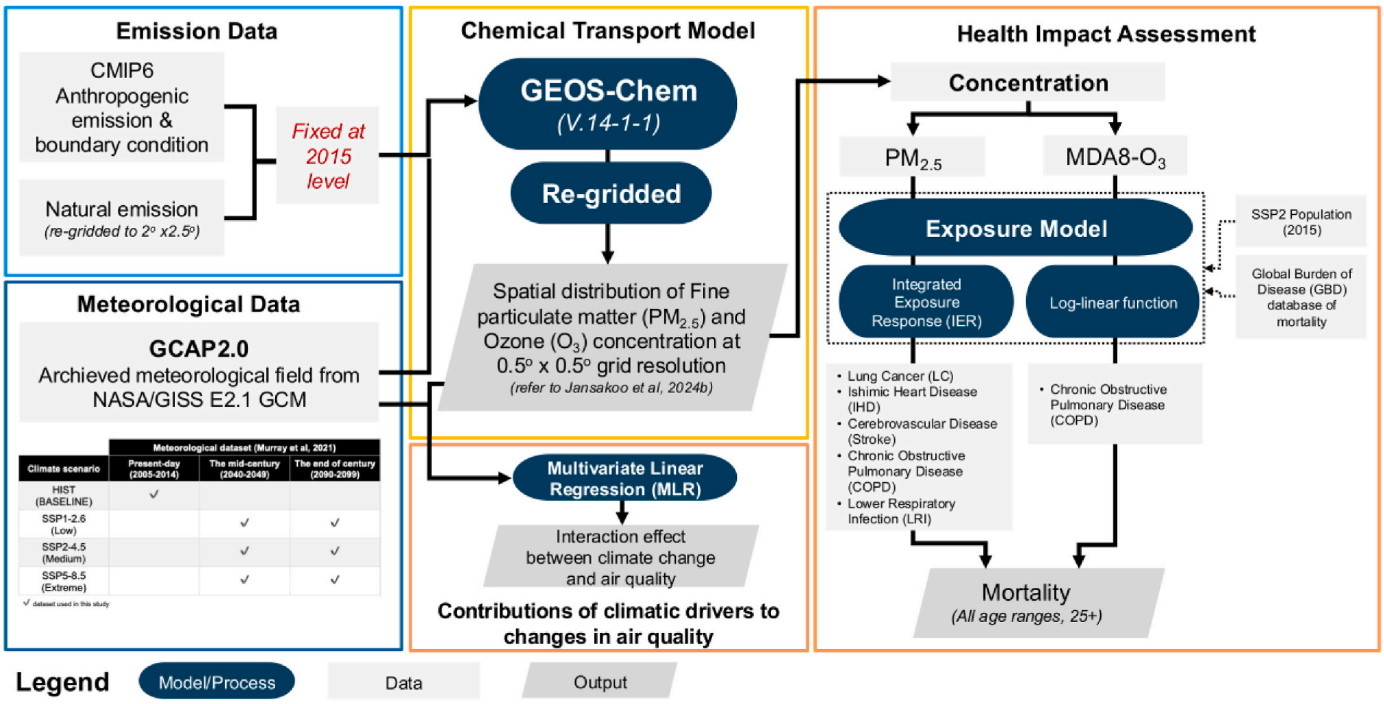

Fig. 1. Overall research framework of this study.

estimates of air pollutant concentration or its health impact assessment. A previous study indicated that, although localized differences may emerge at finer resolutions, regional averages, spatial patterns, and long-term trends remain largely consistent between coarse- and fine-resolution simulations. Given that our study focuses on global and regional analyses under future climate scenarios rather than on local air pollution estimations. Additionally, the computational resources required for multi-scenario, multi-year simulations under climate change pathways make the native 4° x 5° configuration a practical and widely adopted choice within the GEOS-Chem. Following established practice, we then re-gridded the simulated $PM_{2.5}$ and O_3 concentration to 0.5° x 0.5° prior to calculating population-weighted exposure and premature mortalities, consistent with previous studies (Jansakoo et al., 2024a, 2024b; Park et al., 2024b; Uchida et al., 2025). This resolution was chosen to assess the global-scale spatial distribution of air quality under different climate scenarios.

GCAP2.0 is an updated meteorological dataset that builds on the original GCAP framework (Wu et al., 2007). The latest version was developed using outputs of the NASA Goddard Institute for Space Studies (GISS) GCM version E2.1 (Kelley et al., 2020; Murray et al., 2021). GCAP2.0 meteorological fields are provided at a resolution of 2° latitude x 2.5° longitude in 40 vertical layers that are fully compatible with GEOS-Chem. The data are publicly available at http://atmos.earth.rochester.edu/input/gc/ExtData.

GCAP2.0 spans a broader temporal range than formerly, including 1851–1860 (pre-industrial), 2001–2014 (recent past), 2040–2049 (mid-century), and 2090–2099 (end-of-century), and therefore supports future-climate studies well (e.g., Fang et al., 2013; Nazarenko et al., 2015; Pye et al., 2009). The dataset archives hourly two-dimensional fields (e.g., surface temperature, precipitation, wind) and three-hourly three-dimensional fields, always maintaining structural consistency with the MERRA-2-reanalyzed weather data of the NASA Global Modeling Assimilation Office (Murray et al., 2021).

In this study, we used the climate scenario projections of the Scenario Model Intercomparison Project (ScenarioMIP) for CMIP6 (O'Neill et al., 2016). The GCAP2.0 datasets include the meteorologies of seven future climate scenarios from ScenarioMIP: SSP1-1.9, SSP1–2.6, SSP2–4.5, SSP3-7.0, SSP4-3.4, SSP4-6.0, and SSP5–8.5, covering a range of events from aggressive mitigation to high warming.

2.2. Experimental design

We used the SSP1–2.6, SSP2–4.5 and SSP5–8.5 scenarios to represent the low, medium and high climate conditions of Tier 1 of ScenarioMIP (hereafter, SSP–RCP). The anthropogenic emissions and boundary conditions of CMIP6 and GCAP2.0 have been summarized by Riahi et al. (2017) and Gidden et al. (2019). The future meteorological conditions of GCAP2.0 were those of Murray et al. (2021), who described all datasets used for the simulations of the present study.

In brief, SSP1–2.6 considers a low climate impact with aggressive greenhouse gas mitigation and projects an average temperature rise of 1.8 °C by the end of the century. SSP2–4.5 is a "middle-of-the-road" scenario, with a moderate climate impact and an average global temperature rise of 2.7 °C by the end of the century. Lastly, SSP5–8.5 represents an extreme climate scenario, with the highest estimated rise in global mean temperature (4.4 °C) by the end of the century. Future scenarios were simulated for two periods: 2040–2049 (mid-century) and 2090–2099 (end-of-century). The spatial distributions of key meteorological changes (e.g., surface temperature, precipitation, and wind speed) are shown in Fig. A1–A6.

The baseline scenario was the HIST scenario of the present-day meteorology from 2005 to 2014 (denoted BASELINE). Global air-quality evaluations under the SSP–RCPs relative to the BASELINE sought to investigate changes in $PM_{2.5}$ and O_3 levels compared to the past. Table 1 illustrates the overall experimental setup, thus the climate scenarios, and the meteorology and emission matrices used.

In terms of the emission inventories, we assumed no changes in anthropogenic or natural emissions, and no changes in the chemically prescribed upper-atmospheric boundary conditions (e.g., ozone and oxidants) supplied by the GCAP2.0 fields. This experimental design followed that of previous studies using CTMs (Andersson and Langner, 2007; Nolte et al., 2018; L. Yang et al., 2023) in which emissions were held invariant to isolate the impacts of climate change. Accordingly, the $PM_{2.5}$ and O_3 precursor concentrations were fixed at 2015 levels.

The anthropogenic emissions and chemical boundary conditions were taken from the CMIP6 inventory and served as defaults in the

Table 1
Experiment setup of emission and meteorology in this study.

Climate scenario name	Emission year	Meteorological condition year		
		Present-day	Mid-century	End-of-century
HIST (BASELINE)	2015	2005-2014	-	-
SSP1-2.6 (low)	2015	-	2040-2049	2090-2099
SSP2-4.5 (Intermediate)	2015	-	2040-2049	2090-2099
SSP5-8.5 (Extreme)	2015	-	2040-2049	2090-2099

GCAP2.0 framework. These datasets have been archived in the Harmonized Emissions Component (HEMCO) described by Murray et al. (2021). Natural emissions were also held at 2015 levels. We used offline emission levels that had been pre-processed and re-gridded to match the 2.0° x 2.5° horizontal resolutions of the meteorological fields. The offline emissions include dust (Zender et al., 2003), biogenic volatile organic compounds (BVOCs) (Guenther et al., 2012), sea salt and "SeaFlux" (Gong, 2003; Nightingale et al., 2000a, 2000b), and soil NO_x (Hudman et al., 2012). We note that this approach does not account for the meteorological dependence of natural emissions, but it was adopted to minimize additional uncertainties and to isolate the effects of climate-driven meteorological changes on air quality. We acknowledge that meteorology-dependent variations in natural emissions can influence $PM_{2.5}$ and O_3 concentrations, particularly at regional scales; however, such feedbacks are beyond the scope of this study.

In this study, the reactive halogen chemistries of sea salt and organohalogens were excluded because we focused on only meteorological influences without any confounding effect of halogen-driven O_3 loss. The spatial distributions of the fixed 2015-level emissions used are illustrated in Fig. A7.

2.3. Climate impact assessment

2.3.1. Climate-driven changes in $PM_{2.5}$ and O_3 levels

To quantify long-term changes in global air quality, we assessed variations in the 10-year averages of $PM_{2.5}$ and O_3 concentrations driven by the SSP–RCP climate scenarios relative to those simulated under BASELINE (present-day) meteorological conditions. The spatial distributional changes in global $PM_{2.5}$ and peak maximum daily 8-h ozone (PMDA8 O_3) were calculated as decadal averages for the mid-century (2040–2049) and end-century (2090–2099) periods under each SSP–RCP scenario. Hereafter, we use the term "O_3" exclusively to denote PMDA8 O_3. The changes were then re-gridded into a horizontal 0.5° to 0.5° latitude-longitude grid following Jansakoo et al. (2024b). Changes in $PM_{2.5}$ and O_3 concentrations were calculated using Equation (1):

$$\Delta C_{ssp,i} = C_{ssp,i} - C_{base,i} \quad (1)$$

where $\Delta C_{ssp,i}$ is the decadal averaged concentration change in $PM_{2.5}$ in μg m^{-3} and in O_3 in ppbv at grid *i*; $C_{ssp,i}$ denotes the 10-year average concentrations of $PM_{2.5}$ and O_3 under future climate scenarios (i.e., SSP1–2.6, SSP2–4.5, and SSP5–8.5) (*ssp*) at grid *i*; and $C_{base,i}$ are the decadal averaged concentrations of $PM_{2.5}$ and O_3 under the present-day climate scenario (*base*) at grid *i*.

2.3.2. Meteorological evaluation and sensitivity analysis of $PM_{2.5}$ and O_3

The GEOS-Chem model has been extensively evaluated against surface observations for $PM_{2.5}$ and O_3 in numerous previous studies, demonstrating good performance in reproducing present-day pollutant concentrations (e.g., Dang et al., 2021; Hu et al., 2018; Jansakoo et al., 2024b). In this study, emissions and chemical mechanisms are not modified and follow CMIP6-compliant inventories (Murray et al., 2021); therefore, uncertainties in the simulated pollutant responses primarily arise from the meteorological fields used to drive the model.

Before applying GCAP2.0 meteorological fields in GEOS-Chem, we evaluated whether key meteorological variables driving long-term $PM_{2.5}$ and O_3 responses–namely surface temperature and precipitation–are reasonably represented in GCAP2.0 by comparing them with the MERRA-2 reanalysis for the historical period (2005–2014), thereby ensuring that the imposed climate perturbations behave in a physically consistency. This assessment provides confidence that GCAP2.0 captures the large-scale spatial and regional patterns necessary for diagnosing climate-driven air-quality responses. The evaluation approach and results are presented in the next section.

We then identified six meteorological variables relevant to $PM_{2.5}$ and O_3 formation, removal, and transport (Table 2), following the framework of Tai et al. (2010). To confirm their statistical relevance, we calculated Pearson correlations between each variable and pollutant concentrations using historical data (2005–2014). The results shown in Fig. A11 illustrate the grid-based multivariate linear regression relationships between pollutants and meteorological variables, indicating the significance and direction of each pollutant–meteorology relationship.

We next performed grid-based sensitivity analysis to explore how specific meteorological variables influenced changes in $PM_{2.5}$ and O_3 concentrations under different future climate conditions. This isolated the effects of key meteorological drivers on pollutant levels, affording insights into the predominant climate-related factors that shape air-quality responses across scenarios, regions, and seasons.

Unlike previous studies (e.g., Westervelt et al., 2016), which estimated the sensitivity of $PM_{2.5}$ levels to meteorological variables using internal correlations within a single future scenario (e.g., RCP8.5), we focused on the differences between future and historical periods. We calculated the changes in $PM_{2.5}$ and O_3 concentrations between each SSP–RCP scenario and the historical baseline (HIST) and related these to corresponding changes in meteorological drivers. Such a difference-based approach allowed us to isolate long-term climate--driven effects on air quality with emissions held constant. This better represents how future meteorological changes alone may drive variations in $PM_{2.5}$ and O_3 levels.

To quantify these relationships, we used a multivariate linear regression approach adapted from Tai et al. (2010) [Equation (2)]:

$$\Delta C = \beta_0 + \sum_{i=1}^{6} \beta_i \Delta M_i + interaction\ term \quad (2)$$

where ΔC is the annual anomaly in terms of $PM_{2.5}$ (μg m^{-3}) or O_3 (ppbv) (the difference from the 10-year mean relative to that of BASELINE) and ΔM_i is the annual anomaly of the meteorological variable *i*. The term β_i is the standardized regression coefficient (the slope) for variable *i* that quantifies the sensitivity of a pollutant concentration to a unit change in the respective meteorological driver. β_0 is the regression intercept.

Note that the regression coefficients represent the statistically significant sensitivities of $PM_{2.5}$ and O_3 concentrations under the assumption that all other variables are constant. Positive (negative) coefficients indicate that increases (decreases) in the corresponding meteorological variable are associated with increases (decreases) in pollutant

Table 2
Meteorological variables used in this study for $PM_{2.5}$ and O_3 sensitivity analysis.

Variable	Meteorological parameter	Unit
T	Surface temperature at 2 m	°C
PREC	Precipitation	mm d^{-1}
WS[a]	Surface wind speed at 10 m	m s^{-1}
SWGDN	Shortwave radiation	W m^{-2}
RH	Relative humidity	%
CLDTOT	Cloud fraction	unitless

[a] WS is calculated from western wind (U10M) and southern wind (V10M).

concentrations.

2.3.3. Assessment of health impacts

We examined how human health was affected by air-quality variations induced by climate change in terms of the numbers of deaths on the global and regional scales of the Asia-Pacific Integrated Model (AIM-hub). To ensure consistently reliable mortality estimates, particularly for small countries where uncertainties could introduce errors, the original 17 AIM regions were combined into 11 broader regions. This enhanced clarity and transparency. The details are provided in Table A2.

We considered health impacts using the integrated exposure-response (IER) relative risk function of Burnett et al. (2014) for $PM_{2.5}$ and the log-linear function (Malashock et al., 2022) to assess the O_3 mortality relative risk, with uncertainty characterized using 95% confidence intervals. Health impacts were calculated for adults aged 25 years and older (25+). This age group was selected to reflect adult populations typically represented in long-term cohort studies underlying the exposure–response functions. We assumed the same gridded exposure of population data (based on SSP2) across all scenarios (Jones and O'Neill, 2016). For all simulations, we applied a fixed gridded population for the year 2015 using the SSP2 dataset. SSP-based population products represent the best available and most widely adopted gridded population datasets for global climate–air quality assessments and are consistent with the CMIP6 framework underpinning the GCAP2.0 meteorology and emissions. Employing a single, internally consistent population dataset across historical and future simulations allows us to isolate meteorology-driven air-quality changes without introducing inconsistencies arising from population data sources. This isolated the effect of climate change on global air-quality-induced premature mortality (Fang et al., 2013). Equation (3) was used to estimate mortality attributable to $PM_{2.5}$ and O_3 exposure:

$$\Delta \mathrm{Mort}_{i,j} = \left[\mathrm{RR}_j(\mathrm{C}_i) - 1 \,/\, \mathrm{RR}_j(\mathrm{C}_i)\right] \times \mathrm{Pop}_i \times \mathrm{y}_{0_j} \quad (3)$$

where $\mathrm{Mort}_{i,j}$ is the mortality caused by long-term exposure to $PM_{2.5}$ and MDA8 O_3 for region i and disease j; C_i denotes the concentration of $PM_{2.5}$ ($\mu g\ m^{-3}$) and MDA8 O_3 (ppbv) in region i; RR_j is the relative risk of disease j endpoints associated with C_i; Pop_i is the SSP2 population in region i; and y_{0j} is the baseline mortality rate from disease j by country in the Global Burden of Disease (GBD) study.

For $PM_{2.5}$ mortality, the relative risks (RRs) were derived from the IER model that estimates mortality from cerebrovascular disease (stroke), lung cancer (LC), ischemic heart disease (IHD), chronic obstructive pulmonary disease (COPD), and lower respiratory infection (LRI) associated with changes in $PM_{2.5}$ concentrations caused by climate change during both periods. Following the IER model (Burnett et al., 2014), we adopted a lower concentration cutoff (C_0) of 7.5 $\mu g\ m^{-3}$, below which long-term mortality risks were not quantified due to limited epidemiological evidence at the time of IER model development. Equation (4) gives the RRs for $PM_{2.5}$ mortality:

$$\mathrm{RR}_{\mathrm{IER}j}(\mathrm{C}_i) = 1 + \alpha(1 - \exp(-\beta(C_i - C_0)^{\delta})) \quad (4)$$

where α, β, and δ are the IER constants of age and the specific disease j (Burnett et al. 2014); and C_0 is the threshold concentration (the details are in Table A1).

To estimate O_3 mortality, each long-term projection of the hourly ground-level O_3 concentration was calculated as the peak seasonal (6-month) maximum daily 8-h average (MDA8) for each period across all scenarios, and the RRs were estimated using the log-linear function (RR_{log}) of Equation (5). O_3 mortality was considered only for COPD, in line with the GBD study.

$$\mathrm{RR}_{\log j}(\mathrm{C}_i) = \exp\left[((\mathrm{MDA8} - \mathrm{TMREL}) \times \beta) - 1\right] \quad (5)$$

where $\beta = 0.007696$ is the COPD exposure coefficient of Turner et al. (2016) and TMREL = 32.4 ppb (Malashock et al., 2022).

We noted that a theoretical minimum risk exposure level (TMREL) of 32.4 ppbv for O_3, following the GBD study of Malashock et al. (2022). The TMREL represents the concentration below which no additional long-term mortality risk is assumed, and therefore only O_3 increments above this level contribute to the estimated mortality burden.

3. Results

3.1. Changes in global $PM_{2.5}$ and O_3 concentrations

In terms of the spatial distributions, our simulations projected that climate change will increase surface $PM_{2.5}$ levels over tropical regions and the Southern Hemisphere but decrease them across parts of the Northern Hemisphere in both periods (Fig. 2a). This is consistent with the findings of Westervelt et al. (2016), who highlighted the climate-related benefits of increased precipitation in terms of reducing $PM_{2.5}$ levels by the end of the century. We additionally found that the pattern changes in $PM_{2.5}$ levels were possibly attributable to changes in sulfate, nitrate, and ammonium (SNA) levels (Fig. A8). In particular, sulfate levels tended to increase globally by the end of the century under SSP2–4.5 and SSP5–8.5, but to decline under SSP1–2.6. In contrast, both nitrate and ammonium concentrations were projected to decline globally across all SSP–RCP scenarios. These contrasting trends imply that climate-driven changes in chemistry and meteorology may influence the formation and distribution of $PM_{2.5}$ components.

In terms of spatial surface O_3 (Fig. 2b), increases over land were observed in many regions, including parts of China, the Middle East, South America, and Africa, attributable to high emissions of precursors such as NOx and VOCs under favorable meteorological conditions. However, decreases in O_3 levels over other regions (e.g., India, the former Soviet Union [FSU], and North America) and the oceans were clearly observed, particularly under the end-of-century climate conditions. This land-ocean contrast is broadly consistent with that observed in previous studies (e.g., Lam et al., 2011; Murray et al., 2024; Zanis et al., 2022) that reported similar spatial patterns under future climate conditions, implying that regional responses may be more complex than previously recognized, being potentially influenced by localized meteorological or chemical conditions.

The spatial distributions of climate-driven changes in seasonal $PM_{2.5}$ and O_3 concentrations exhibited clear seasonal dependencies across all SSP–RCPs (Figs. A9 and A10). For $PM_{2.5}$, the highest global shifts were observed during the JJA and DJF seasons and exceeded 0.1 $\mu g\ m^{-3}$ under SSP5–8.5 at the end of the century. SSP1–2.6 and SSP2–4.5 exhibited similar seasonal $PM_{2.5}$ patterns, but the changes were smaller, particularly over North Africa and parts of Europe. In contrast, during the MAM and SON seasons, changes in annual global $PM_{2.5}$ levels were lower than those projected under DJF and JJA.

O_3 concentrations also exhibited notable seasonal variations (Fig. A10). Although the global mean changes generally declined, especially over oceans, the surface O_3 levels over land exhibited distinct seasonal patterns. An increase in O_3 was observed during the JJA and SON seasons across most SSP–RCPs, particularly over land in the Northern Hemisphere. In contrast, the MAM season exhibited consistent decreases in O_3 across many regions, especially North America, but slight increases in certain localized areas. These findings highlight the critical roles played by seasonal meteorological conditions (temperature, precipitation, solar radiation, and atmospheric circulation) in terms of the formation, transport, and removal of air pollutants under future climate scenarios.

In terms of the mean changes in $PM_{2.5}$ (Fig. 3a), by mid-century, global mean $PM_{2.5}$ values decreased by −0.31 $\mu g\ m^{-3}$, –0.19 $\mu g\ m^{-3}$, and –0.21 $\mu g\ m^{-3}$ under SSP1–2.6, SSP2–4.5, and SSP5–8.5, respectively. By the end of the century, $PM_{2.5}$ levels continued to decline, (especially under SSP1–2.6 with the largest decrease of −0.57 $\mu g\ m^{-3}$). The changes differed across the scenarios, driven by distinct meteorological shifts. At the regional level, decreases of–0.2 $\mu g\ m^{-3}$ or more

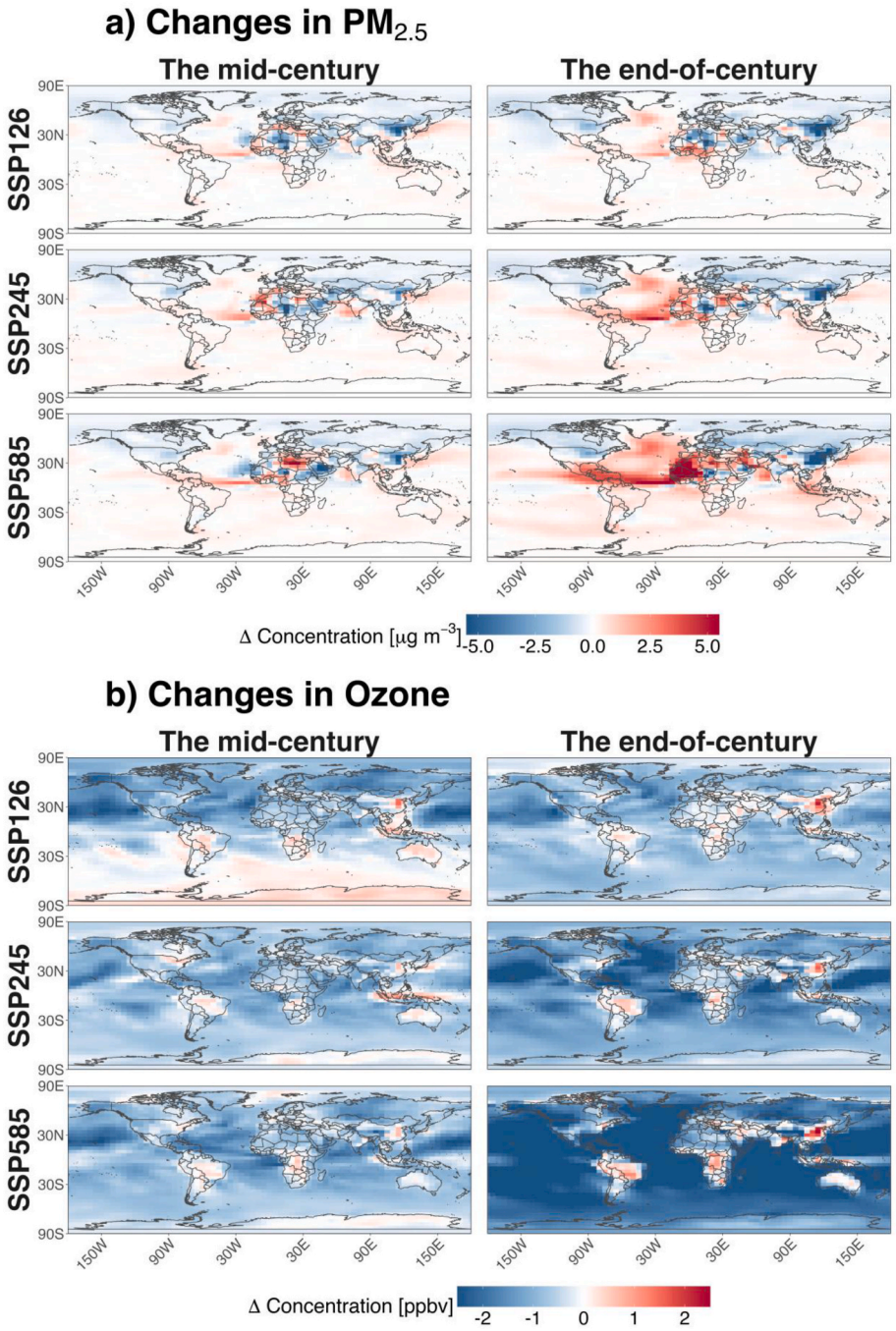

Fig. 2. Spatial distribution changes of global concentration in the mid-century (2040-2049) and the end of century (2090-2099) periods (from left to right) due to climate change under SSP1-2.6, SSP2-4.5 and SSP5-8.5 relative to BASELINE for $PM_{2.5}$ in μg m^{-3} (a); and Ozone in ppbv (b). See the $PM_{2.5}$ composition changes in Sulfate, Nitrate, and Ammonium (SNA) in the supplementary materials.

were observed, especially for China, the Middle East, North America, the FSU, and Europe, under both timeframes. In contrast, South America exhibited increased $PM_{2.5}$ concentrations under all SSP–RCP scenarios, ranging from +0.01 to +0.86 μg m^{-3}.

In terms of the mean change in O_3 (Fig. 3b), decreases in surface levels were observed globally and across most regions. Reductions of −0.05 ppbv or more were projected in many areas. This downward trend was consistent across the scenarios, and particularly evident toward the end of the century, with SSP1–2.6 showing a modest decline (−0.38 ppbv), but SSP2–4.5 (−0.69 ppbv) and (especially) SSP5–8.5 (−1.20 ppbv) showing greater declines. The spatial patterns (Fig. 2b) revealed both increases and decreases, but the global and regional means were net reductions, reflecting widespread O_3 loss driven by climate-induced increases in humidity and temperature.

3.2. *Evaluation of GCAP2.0 meteorology and sensitivity of $PM_{2.5}$ and O_3*

3.2.1. *Evaluation of GCAP2.0 meteorological fields*

The GCAP2.0 meteorological fields were evaluated by comparing surface temperature (T) and precipitation (PREC) against the MERRA-2 reanalysis for the historical period (2005–2014) (Fig. 4a–d).

Surface temperature from GCAP2.0 reproduced the large-scale spatial patterns with strong agreement over both land and ocean (R = +0.99). Warm biases were found primarily over the Northern

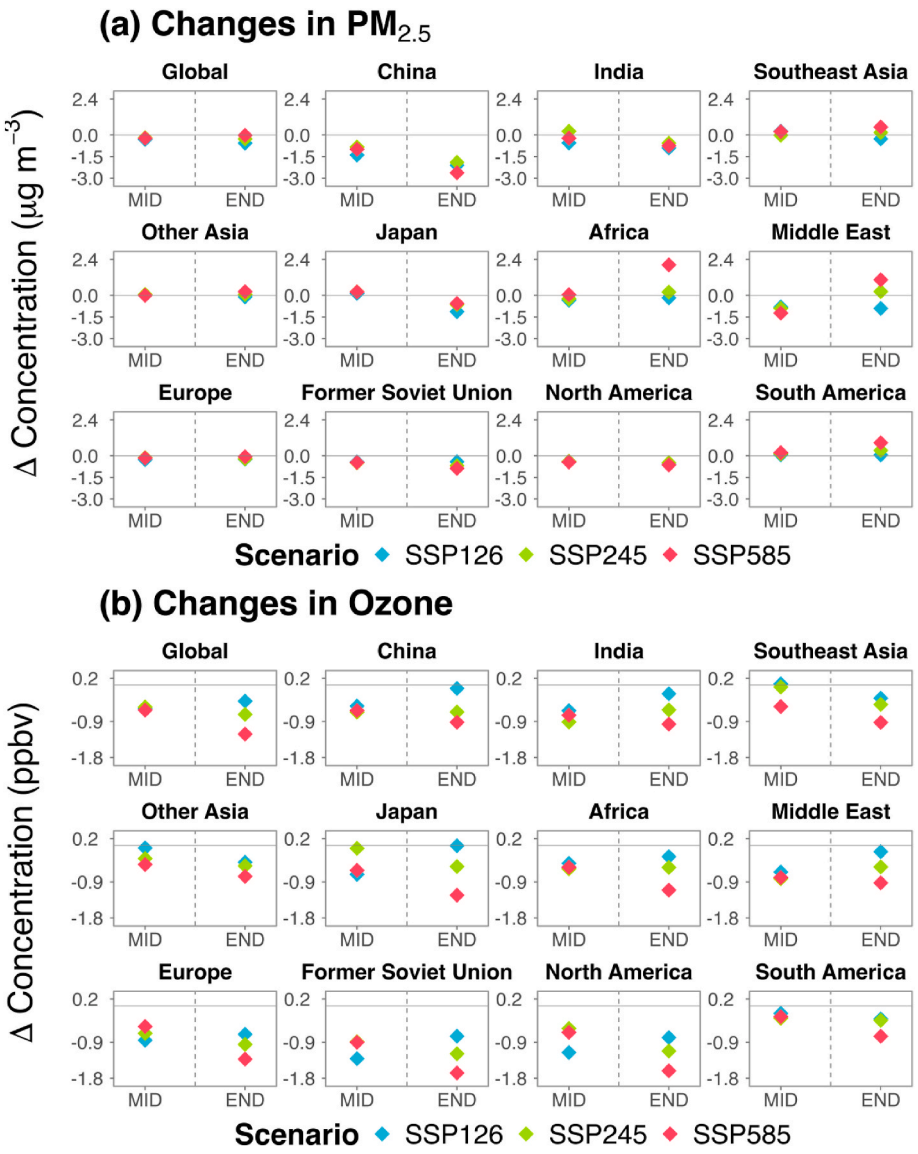

Fig. 3. Mean of global and regional surface $PM_{2.5}$ concentration (a) and peak daily maximum 8-h ozone (PMDA8 O_3) concentration (b) during the mid- (MID) and end- (END) century relative to the BASELINE.

Hemisphere oceans and high-latitude regions, consistent with previous evaluations of GCAP2.0 and other free-running GCMs. These warm deviations are expected because GCAP2.0 inherits the radiative and cloud parameterizations of the GISS-E2-1-G model, whose radiation code and lack of data assimilation can lead to slightly higher temperatures than MERRA-2 (Murray et al., 2021). Over land, temperature biases were generally small across most regions (e.g., North America, Europe, Japan, China, and the Former Soviet Union), where the interquartile ranges remained narrow, indicating robust agreement with MERRA-2. More pronounced warm biases occurred mainly in polar-influenced high--latitude regions and parts of the Southern Hemisphere, reflecting known characteristics of GCM temperature fields.

For precipitation, GCAP2.0 captured the broad spatial patterns but exhibited weaker agreement with MERRA-2 than temperature. Correlations were higher over the oceans ($R = +0.81$) than over land ($R = +0.73$), reflecting the smoother large-scale variability of oceanic precipitation and the greater heterogeneity of land-based precipitation processes. Moderate wet biases appeared across many land regions, including parts of North America, Europe, and Asia, while dry biases were more pronounced in high-latitude regions and portions of the Southern Hemisphere oceans. In addition, GCAP2.0 produced higher precipitation over oceanic regions near the Intertropical Convergence Zone (ITCZ) than MERRA-2, a pattern consistent with the known tendency of GCM convective parameterization schemes to overestimate precipitation in the tropics (Murray et al., 2021).

3.2.2. *Sensitivity of climate-driven meteorological changes in global $PM_{2.5}$ and O_3 levels*

The GEOS-Chem simulations do not include climate-chemistry feedback. We therefore quantified the sensitivities of global $PM_{2.5}$ and O_3 levels to changes in six key meteorological variables using the multiple linear regression model described in Section 2.3.2. Overall, the sensitivity patterns revealed that surface $PM_{2.5}$ and O_3 concentrations responded to meteorological drivers in a spatially consistent manner across the scenarios. However, the direction (sign) and the magnitude of the response depended on the climate conditions of each SSP–RCP. The climate dynamics and pollutant sensitivities differed regionally.

Fig. 5 shows the spatial distributions of the regression coefficients for global $PM_{2.5}$, indicating the directions and magnitudes of the sensitivities with respect to changes in temperature and precipitation. The sensitivities to the remaining meteorological variables are provided in Fig. A12, which shows consistent spatial patterns but with weaker or

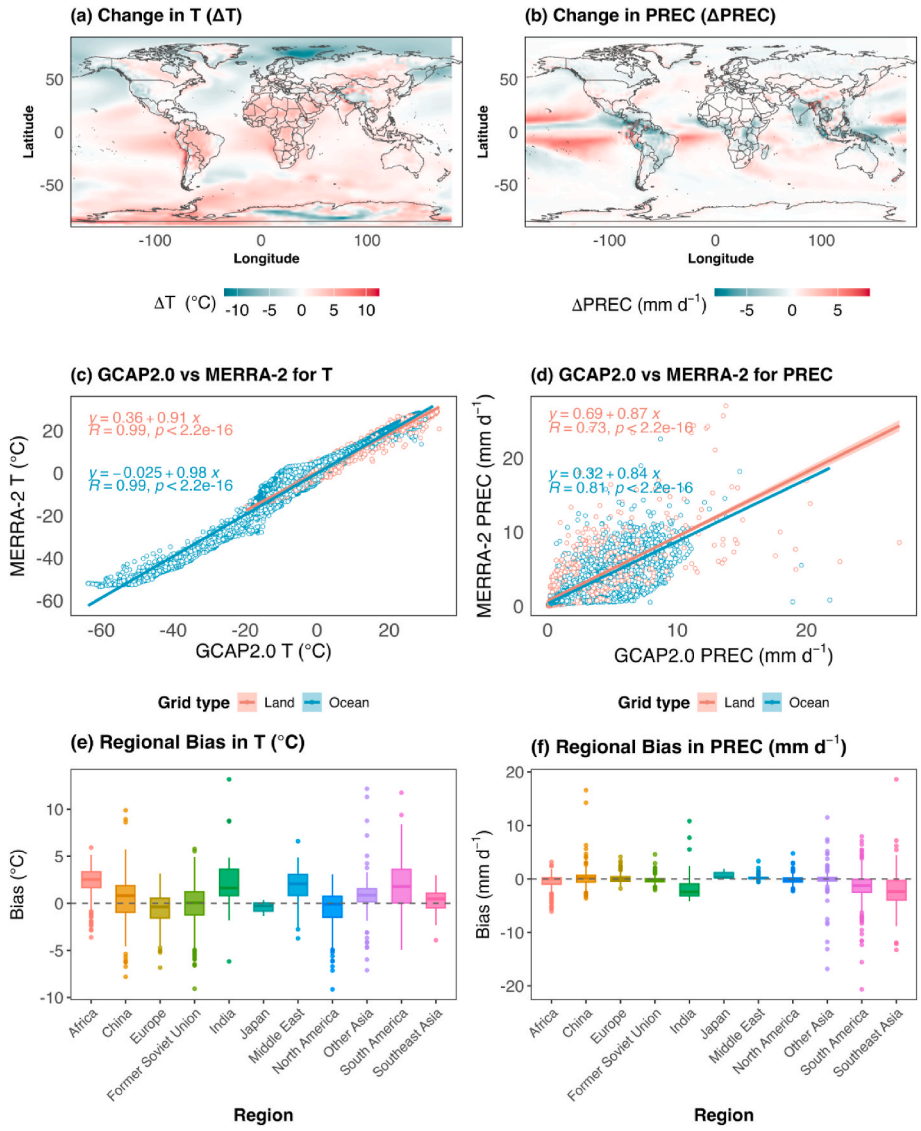

Fig. 4. Evaluation of surface temperature (T) and Precipitation (PREC) fields in GCAP2.0 against MERRA-2 for the historical data (2005-2014). (a–b) Spatial distribution change of GCAP2.0 relative to MERRA-2. (c–d) Grid-based scatterplots comparing GCAP2.0 and MERRA-2. Colors indicate land and ocean points. Pearson correlation coefficients and linear regression equations are shown for each type. (e–f) Regional distributions of GCAP2.0–MERRA-2 biases. Boxes represent the interquartile range, horizontal lines denote the median, and whiskers show variability across regions. Positive values indicate that GCAP2.0 exceeds MERRA-2.

more localized responses. Table 3 summarizes the average global responses. Overall, $PM_{2.5}$ levels were positively sensitive to surface temperature ($\Delta PM_{2.5}/\Delta T$) over both time frames, indicating that warming was associated with enhanced $PM_{2.5}$ levels, likely reflecting the combined influence of temperature-driven secondary aerosol formation and regionally dependent changes in precipitation and wet deposition processes. The greatest temperature responses were those under SSP2–4.5 ($+0.073\ \mu g\ m^{-3}$) and SSP5–8.5 ($+0.072\ \mu g\ m^{-3}$) at mid-century. Precipitation exhibited negative sensitivities across all scenarios under both periods; wet scavenging removes pollutants. The largest effect was that under SSP5–8.5 at mid-century ($-0.783\ \mu g\ m^{-3}$). Increased wind speeds also exerted a consistently negative influence, especially under SSP2–4.5 at the end of the century ($-0.04\ \mu g\ m^{-3}$), implying more effective pollutant dispersion. $PM_{2.5}$ likely responded positively to the cloud fraction, especially under SSP2–4.5 and SSP5–8.5 at the end of the century, with increases of more than $+0.07\ \mu g\ m^{-3}$, possibly attributable to suppressed photochemical activity and decreased boundary-layer mixing under high cloud. The influence of shortwave radiation was relatively weak, but RH consistently exhibited strong negative sensitivities across all scenarios, particularly under SSP1–2.6 and SSP2–4.5 at mid-century (approximately $-0.07\ \mu g\ m^{-3}$), implying that higher humidity may suppress aerosol formation or promote particle growth beyond the fine fraction. The high explained R^2 values (0.75–0.77) across all cases indicate that the key meteorological drivers covered a substantial proportion of the $PM_{2.5}$ variability under future climate conditions.

O_3 concentrations also demonstrated clear responses to meteorological changes, particularly temperature and RH, with distinct global patterns across the scenarios (Fig. 6 and Fig. A13). Although positive temperature–O_3 relationships have been widely documented in regional studies (Jacob and Winner, 2009; Lou et al., 2015), our global-scale analysis revealed negative associations between O_3 and both temperature and cloud fraction (Fig. A13c). This apparent relationship likely reflects the combined influence of correlated meteorological variables, including cloudiness and relative humidity (Fig. A11), which exert strong suppressive effects on photochemical O_3 formation (Doherty et al., 2013), rather than a direct temperature-driven response alone.

Table 4 lists the surface O_3 changes by variations in the six key meteorological components. Globally, a strong negative sensitivity to temperature change ($\Delta O_3/\Delta T$) was apparent, particularly under

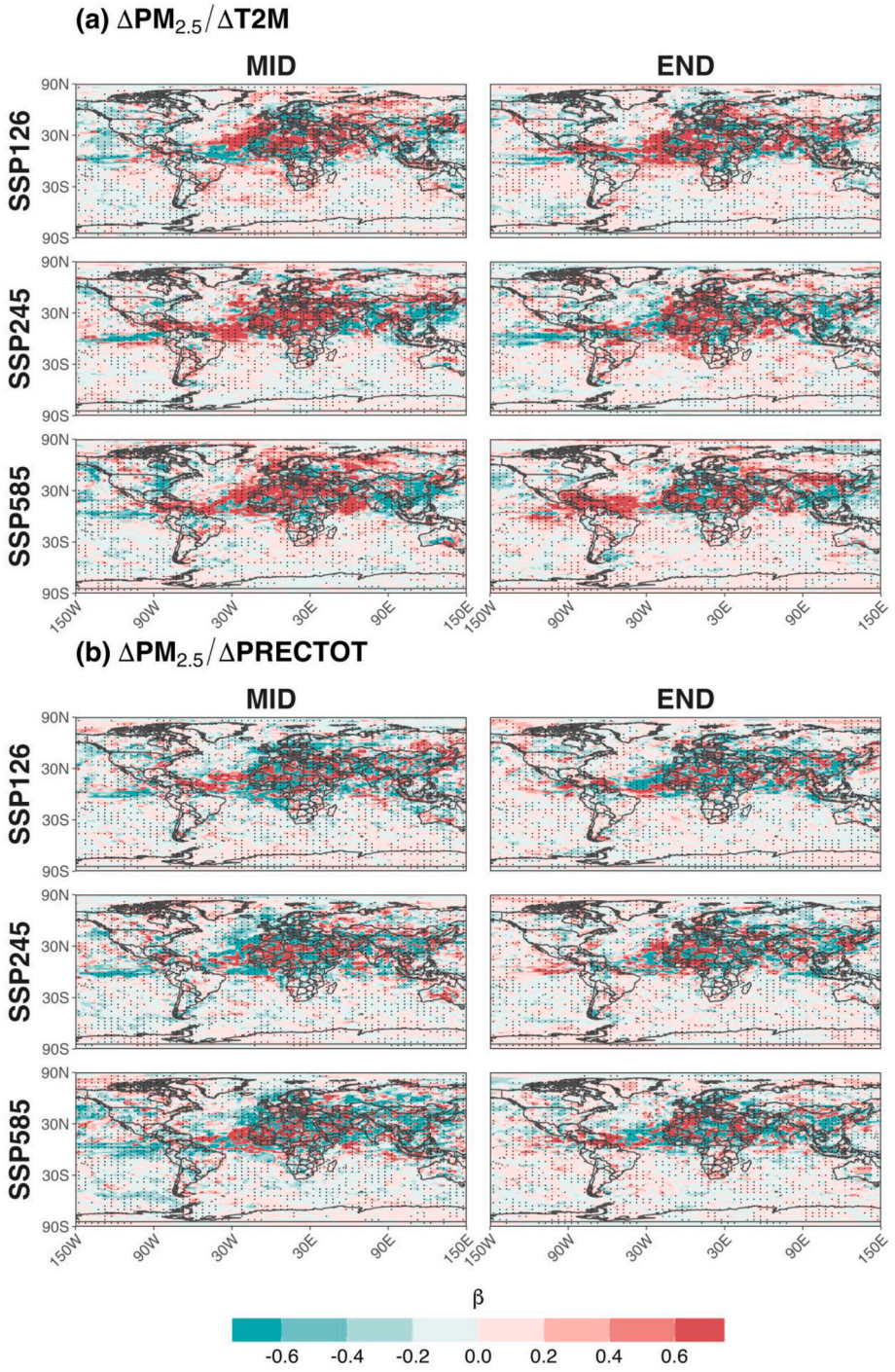

Fig. 5. Spatial distributions of the standardized regression coefficients (β) of changes in $PM_{2.5}$ ($\Delta PM_{2.5}$) with respect to temperature (ΔT) and precipitation (ΔPREC) under SSP1-2.6, SSP2-4.5, and SSP5-8.5 for the mid-century (MID) and end-of-century (END) periods. Dots indicate statistically significant grid cells ($p < 0.05$). Results for other key meteorological variables (WS, RH, CLDTOT, SWGDN) are provided in Fig. A12.

SSP5–8.5 at the end of the century (−0.243 ppbv), followed by SSP2–4.5 (−0.124 ppbv) and SSP1–2.6 (−0.094 ppbv). The RH sensitivity ($\Delta O_3/\Delta RH$) also exhibited consistently strong negative influences across all scenarios, particularly under SSP1–2.6 and SSP5–8.5 at the end of the century (−0.062 and −147 ppbv, respectively). In contrast, the shortwave radiation sensitivity ($\Delta O_3/\Delta SWGDN$) exhibited a consistently positive association with surface O_3 concentrations across all scenarios and timeframes. This was to be expected; more solar radiation enhances photolysis of O_3 precursors such as NOx, thereby accelerating photochemical O_3 production. The effect of the cloud fraction was more variable, with some responses being negative (e.g., −0.022 ppbv under SSP5–8.5 mid-century) and others positive (+0.101 ppbv under SSP5–8.5 at end-century), depending on the scenario and the climate conditions. Although wind speed and precipitation are not direct chemical drivers of O_3 production, indirect effects were evident. Both factors contributed a substantial proportion of the variance in O_3 changes (R^2 up to 0.70), likely because they affected pollutant transport, atmospheric dispersion, and precursor removal via convection and wet deposition (Doherty et al., 2013; Fiore et al., 2012).

Table 3
Summary of global mean standardized regression coefficients with 99% confident interval (CI)and explained variance (R^2) from multiple linear regression between global annual surface $PM_{2.5}$ changes ($\Delta PM_{2.5}$) and six climate-driven meteorological variables (surface temperature (ΔT), precipitation (ΔPREC), cloud fraction (ΔCLDTOT), wind speed (ΔWS), shortwave radiation(ΔSWGDN), and relative humidity(ΔRH)) under SSP1-2.6, SSP2-4.5, and SSP5-8.5 scenarios for the mid-century (2040-2049) and end-of-century (2090-2099) periods.

Region	Scenario	Period[a)]	Regression coefficient [99%CI]						Explained R^2[b)]
			$\Delta PM_{2.5}/\Delta T$	$\Delta PM_{2.5}/\Delta PREC$	$\Delta PM_{2.5}/\Delta WS$	$\Delta PM_{2.5}/\Delta RH$	$\Delta PM_{2.5}/\Delta CLDTOT$	$\Delta PM_{2.5}/\Delta SWGDN$	
Global	SSP1-2.6	MID	0.018 [0.014, 0.021]	−0.053 [-0.057, −0.048]	−0.005 [-0.009, −0.002]	−0.071 [-0.077, −0.064]	0.07 [0.064, 0.077]	−0.021 [-0.027, −0.014]	0.75
		END	0.052 [0.048, 0.055]	−0.026 [-0.029, −0.023]	−0.029 [-0.033, −0.025]	−0.065 [-0.07, −0.059]	0.069 [0.061, 0.076]	0.03 [0.023, 0.038]	0.75
	SSP2-4.5	MID	0.073 [0.069, 0.078]	−0.046 [-0.051, −0.041]	−0.017 [-0.021, −0.013]	−0.067 [-0.068, −0.052]	0.053 [0.046, 0.061]	−0.013 [-0.022, −0.003]	0.76
		END	0.02 [0.016, 0.024]	−0.012 [-0.016, −0.008]	−0.039 [-0.043, −0.035]	−0.03 [-0.036, −0.024]	0.088 [0.079, 0.097]	0.073 [0.062, 0.083]	0.75
	SSP5-8.5	MID	0.072 [0.067, 0.077]	−0.048 [-0.054, −0.042]	−0.022 [-0.027, −0.017]	−0.039 [-0.047, −0.03]	0.056 [0.048, 0.063]	−0.039 [-0.047, −0.031]	0.77
		END	0.061 [0.057, 0.064]	−0.027 [-0.031, −0.023]	−0.01 [-0.014, −0.007]	−0.042 [-0.048, −0.036]	0.071 [0.065, 0.077]	−0.004 [-0.01, 0.003]	0.74

[a)] MID denotes The mid-century; and END denotes The end-of-century.
[b)] R^2 corresponds to the model fit across all grid cells.

3.3. Climate change-induced air-quality impacts on mortality

Fig. 7 shows the mortality changes under future climate scenarios relative to those under the BASELINE condition. The changes are presented both globally and regionally.

In terms of $PM_{2.5}$ mortality (Fig. 7a), regional analysis indicated that global premature deaths attributable to $PM_{2.5}$ exposure by mid-century were projected to decline by −0.032 million deaths under SSP1–2.6, −0.019 million deaths under SSP2–4.5, and −0.017 million deaths under SSP5–8.5. By the end of the century, the estimated reductions in $PM_{2.5}$-related mortality further increased, to −0.078 million deaths under SSP1–2.6, −0.045 million deaths under SSP2–4.5, and −0.014 million deaths under SSP5–8.5. The reduction in $PM_{2.5}$ induced by climate change across all SSP–RCP scenarios decreased deaths, consistent with previous studies conducted using RCP-based climate scenarios (e.g., Silva et al., 2017; West et al., 2013), which also reported climate-driven air-quality improvements and associated health benefits.

At the regional level, the most deaths avoided were in China, India, other Asian countries, the FSU, and Europe, both at the mid-century and the end of the century. Notably, despite having high population densities–which would typically increase vulnerability to pollution-induced health impacts–countries such as China still exhibit substantial net declines in $PM_{2.5}$-related mortality by the end of the century, with −36.4, −31.1, and −43.3 thousand deaths avoided under SSP1–2.6, SSP2–4.5, and SSP5–8.5, respectively. These declines occur because climate-driven reductions in $PM_{2.5}$ concentrations offset the population–related health risks. This implies that climate-related improvements in meteorological conditions (e.g., increased dispersion or precipitation) mitigate air-pollution-related health risks, even in heavily polluted/populated regions. In contrast, increased $PM_{2.5}$-related mortality was observed elsewhere under SSP5–8.5 by the end of the century, with premature deaths rising by up to 20.4 thousand deaths in Southeast Asia and 19.1 thousand deaths in South America. These findings emphasize both the potential benefits of climate mitigation and the uneven, region-specific nature of climate-induced air-pollution risks.

In terms of O_3 mortality, Fig. 7b shows that global average O_3 mortality was projected to decrease under all SSP–RCP scenarios for both periods, except for SSP1–2.6 at the end of the century. By mid-century, global O_3-related premature deaths declined by −0.0006, −0.01, and −0.001 million deaths under SSP1–2.6, SSP2–4.5, and SSP5–8.5, respectively. At the end of the century, global average O_3 mortality fell by −0.004 and −0.006 million deaths under SSP2–4.5 and SSP5–8.5, respectively, but under SSP1–2.6 increased by +0.004 million deaths. This implies that even under the relatively modest warming of SSP1–2.6–considerably lower than the warming projected under SSP2–4.5 and SSP5–8.5–the combination of higher temperatures and other favorable meteorological conditions (e.g., increased solar radiation or stagnation) can still enhance O_3 formation and lead to increases in O_3-related mortality by the end of the century.

At the regional level, O_3-related mortality in most regions was projected to decrease across all SSP–RCP scenarios for both timeframes. In particular, SSP1–2.6 was associated with widespread reductions, particularly in India, Europe, and North America (−3.91, −1.23, and −0.74 thousand deaths by mid-century). Similar patterns were observed under SSP2–4.5 and SSP5–8.5 for the same period, but with greater reductions, reflecting stronger climate-driven benefits. In contrast, China exhibited a divergent pattern. By mid-century, China experienced an increase in O_3-related mortality under SSP1–2.6 (+2.70 thousand deaths) although decreases were apparent under SSP2–4.5 (−1.03 thousand deaths) and SSP5–8.5 (−0.78 thousand deaths). By the end of the century, O_3-related premature deaths in China increased sharply under all scenarios; +3.61 thousand deaths under SSP2–4.5, +7.83 thousand deaths under SSP1–2.6, and +8.20 thousand deaths under SSP5–8.5. This indicates that, even with emissions held constant, climate-induced meteorological changes such as temperature and cloud cover variations may either significantly enhance or suppress O_3 formation, in turn increasing or decreasing the health impacts. Such dynamics can amplify or offset the effects of emission changes, even in regions already at risk of high O_3 levels. The findings underscore the need to consider climate-pollution interactions during future air-quality and health-impact assessments.

To understand the relative roles of climate- and emission-driven changes in air pollution–related mortality, we compared future projections of PM2.5- and O3-attributable deaths with a reference scenario based on SSP2 emissions under fixed present-day climate conditions, hereafter referred to as the BaU case.

This BaU scenario follows the SSP2 (“middle-of-the-road”) pathway, which is the default baseline used in the AIM-Hub framework for constructing consistent global emission trajectories (Fujimori et al., 2017, 2018; Riahi et al., 2017). SSP2 provides balanced assumptions regarding population, GDP, energy use, land-use patterns, and technological development, without strong mitigation or fragmentation trends, making it an appropriate policy-neutral reference scenario.

By excluding climate responses associated with SSP2–RCP pathways (e.g., SSP2–4.5), this design allows the BaU case to represent a meteorology-as-usual reference, thereby enabling a clear separation between emission-driven and climate-driven impacts when compared with the climate-change experiments. Fig. A14 shows the $PM_{2.5}$ and O_3

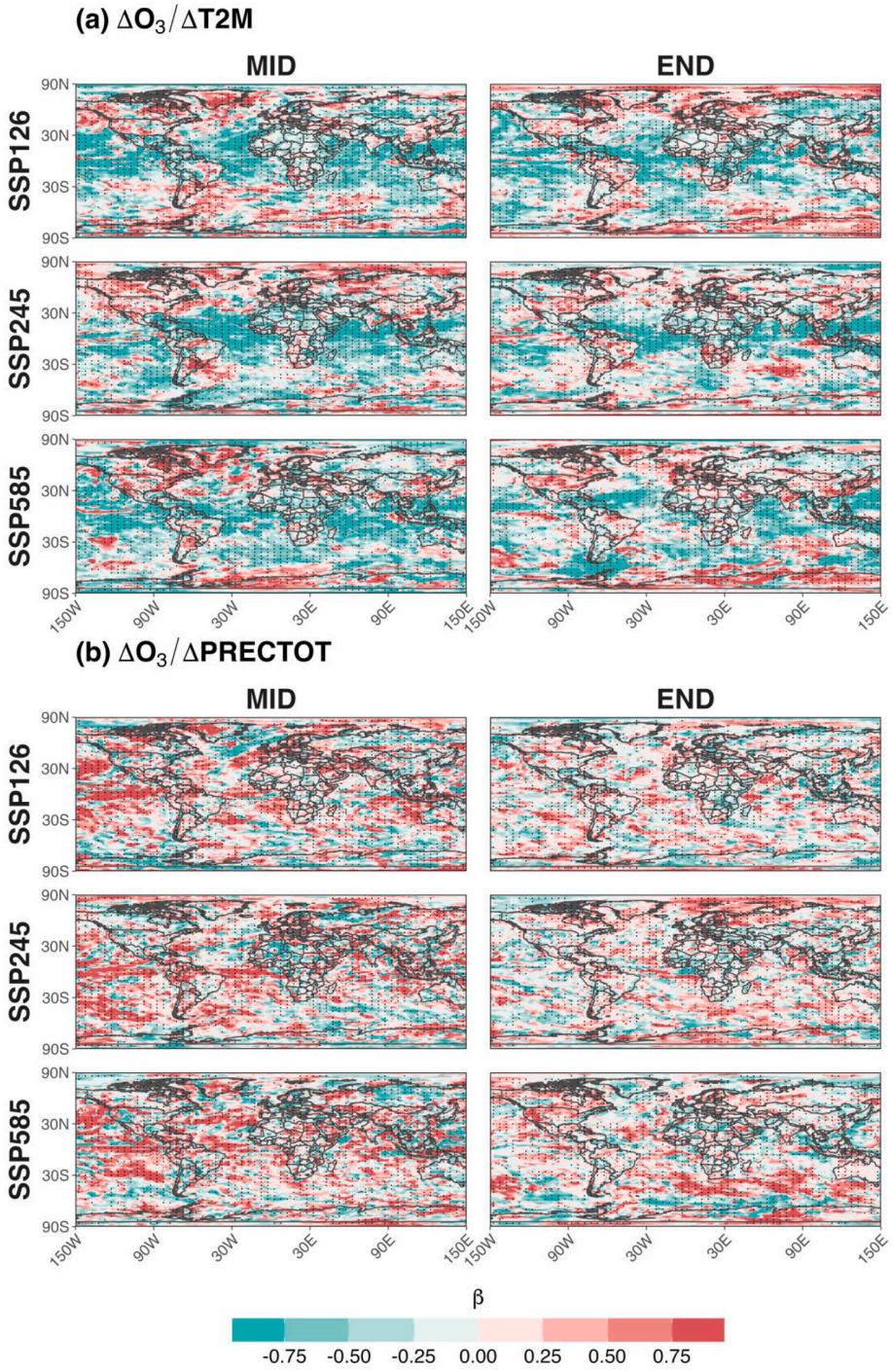

Fig. 6. The same as Fig. 5 but for Ozone (ΔO_3). Results for other key meteorological variables (WS, RH, CLDTOT, SWGDN) are provided in Fig. A13.

precursor emissions under this reference scenario (or BaU). This offers a perspective on how climate-induced meteorological changes alone affect global air-pollution-related health outcomes, independent of emission trends.

Fig. 8 shows the mortality impacts attributable to global $PM_{2.5}$ and O_3 under various climate-driven scenarios (HIST, SSP1–2.6, SSP2–4.5, and SSP5–8.5) compared to the emission-driven scenario (BaU). We found that climate-driven $PM_{2.5}$-related mortality was lower than that of BaU during the present-day and at mid-century (2050s) but became higher than that of BaU by the end of the century (2100), particularly under SSP5–8.5 (+16.1%).

In contrast, climate-driven O_3 mortality was consistently lower than that of the BaU scenario across all scenarios and timeframes, with substantial reductions of approximately −60% by mid-century and −80% by the end of the century. This difference likely reflects the role of methane emission increases under the SSP2-based BaU scenario in enhancing background O_3 concentrations, thereby contributing to higher ozone-related mortality relative to the climate-driven simulations. At the regional scale, increases and/or decreases in $PM_{2.5}$- and O_3-related mortality were observed, particularly in highly populated regions such as China, Japan, and India. These variations emphasize the spatial heterogeneity of climate-driven health outcomes, with particular regions experiencing either a health benefit or penalty depending on the local meteorological responses (Fig. A15).

Table 4
The same as Table 3 but for Ozone (ΔO_3).

Region	Scenario	Period[a)]	Regression coefficient [99%CI]						Explained $R^{2b)}$
			$\Delta O_3/\Delta T$	$\Delta O_3/\Delta PREC$	$\Delta O_3/\Delta WS$	$\Delta O_3/\Delta RH$	$\Delta O_3/\Delta CLDTOT$	$\Delta O_3/\Delta SWGDN$	
Global	SSP1-2.6	MID	−0.208 [-0.212, −0.204]	0.100 [0.096, 0.105]	−0.031 [-0.034, −0.028]	−0.059 [-0.064, −0.055]	−0.068 [-0.074, −0.063]	0.012 [0.007, 0.018]	0.73
		END	−0.094 [-0.097, −0.091]	−0.006 [-0.009, −0.004]	−0.029 [-0.032, −0.026]	−0.062 [-0.065, −0.058]	−0.014 [-0.019, −0.009]	0.03 [0.025, 0.036]	0.75
	SSP2-4.5	MID	−0.154 [-0.158, −0.151]	0.122 [0.118, 0.126]	−0.012 [-0.015, −0.009]	−0.052 [-0.056, −0.047]	0.004 [-0.002, 0.009]	0.074 [0.069, 0.079]	0.75
		END	−0.123 [-0.127, −0.12]	0.044 [0.042, 0.047]	0.026 [0.023, 0.029]	−0.04 [-0.044, −0.036]	−0.083 [-0.088, −0.077]	0.032 [0.038, 0.027]	0.74
	SSP5-8.5	MID	−0.243 [-0.247, −0.24]	0.112 [0.107, 0.116]	0.03 [0.026, 0.033]	−0.047 [-0.052, −0.042]	−0.022 [-0.028, −0.016]	0.046 [0.039, 0.052]	0.74
		END	−0.124 [-0.127, −0.121]	0.044 [0.041, 0.047]	−0.064 [-0.067, −0.061]	−0.147 [-0.151, −0.143]	0.101 [0.096, 0.106]	0.068 [0.064, 0.073]	0.74

[a)] MID denotes The mid-century; and END denotes The end-of-century.
[b)] R^2 corresponds to the model fit across all grid cells.

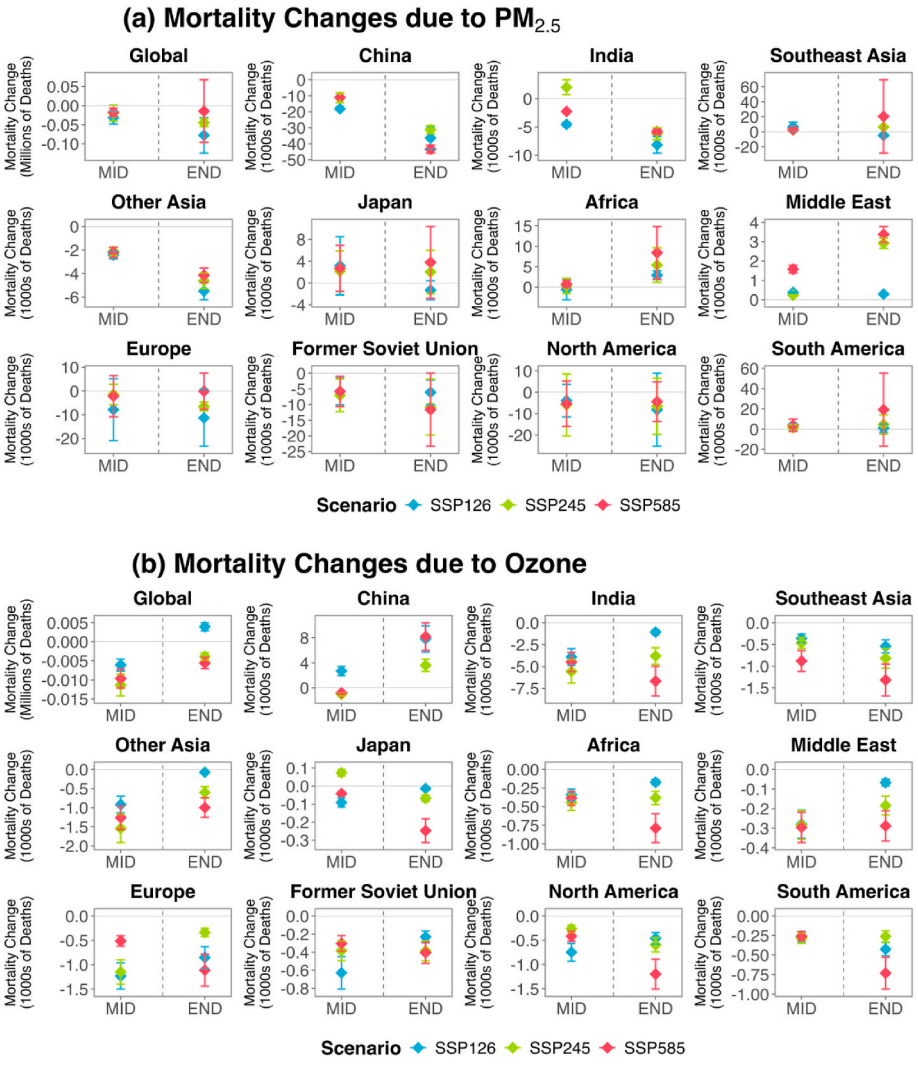

Fig. 7. Global and regional mean changes in $PM_{2.5}$- and O_3-related premature mortality for adults aged 25 years and older (25+) under different climate scenarios. Results are shown for the mid-century (2040–2049) and end-of-century (2090–2099) periods relative to the present day (2005–2014). Error bars indicate 95% confidence intervals.

4. Discussion and limitations

We used GCAP2.0 meteorological fields to drive the GEOS-Chem model under different SSP–RCPs. This estimated the effects of pollutants on future air quality and human health. We found that magnitudes and intensities of the $PM_{2.5}$ and O_3 concentrations depended on the meteorological changes in the SSP–RCP scenarios over both the mid-century and end-of-century time frames (Sections 3.1 and 3.2).

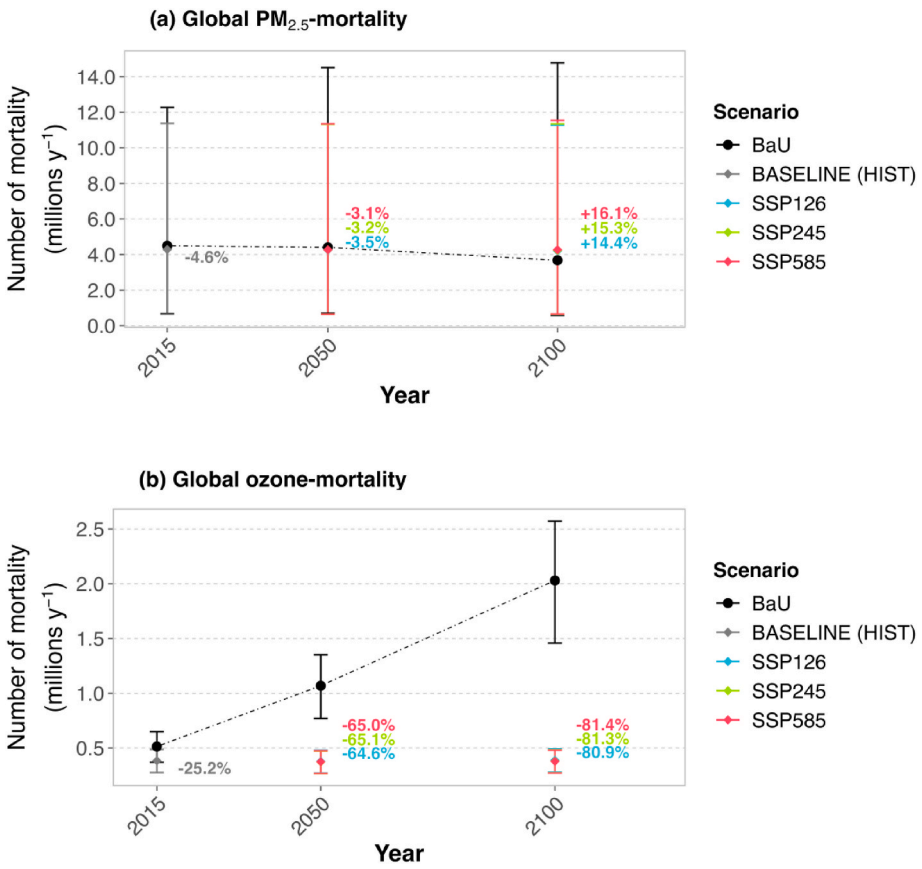

Fig. 8. Projected number of mortality attributable to $PM_{2.5}$ (a) and ozone (b) under climate-driven scenarios (HIST, SSP1-2.6, SSP2-4.5, SSP5-8.5), compared to the emission-driven baseline (BaU). Values represent the relative change in annual mortality (%) between the climate-driven scenarios and BaU. The error bars represent 95% confidence intervals.

It is important to note that these responses reflect meteorological sensitivity rather than projections of future air quality under the SSP–RCP scenarios. In this study, all anthropogenic and natural emissions, and chemical boundary conditions were fixed at 2015 levels; therefore, the simulated concentration changes arise solely from prescribed meteorological perturbations. They do not include the dynamically changing emissions, greenhouse gas trajectories, or atmospheric composition changes that accompany the actual SSP pathways. Thus, processes such as changes in methane, biogenic and wildfire emissions, and aerosol–radiation or aerosol–cloud feedback–each of which would influence $PM_{2.5}$ and O_3 in realistic future projections–are not represented here.

Accordingly, while our results highlight the substantial role of meteorology in shaping pollutant levels, they should not be interpreted as indicating that climate change alone will improve air quality or reduce health burdens. Instead, this study quantifies the isolated effect of climate-driven meteorological changes, providing insight into one component of the broader climate–air quality system. In addition, consistent with previous studies (e.g., Dawson et al., 2007; Doherty et al., 2013), our results show that climate-driven changes in $PM_{2.5}$ and O_3 are highly region-specific and spatially heterogeneous. This pronounced regional to local variability highlights the importance of developing downscaled climate projections to support more robust air-quality assessments and inform effective air-quality and climate policies at national to continental scales.

4.1. *Effects of climate on air quality: patterns and drivers*

4.1.1. *$PM_{2.5}$ projection*

Global average $PM_{2.5}$ concentrations under future climate changes declined across most scenarios, particularly by the end of the century. However, the magnitudes and spatial distributions of such changes were strongly modulated by the regional meteorological variations of the SSP–RCP scenarios. Climate-driven reductions in $PM_{2.5}$ were most pronounced in the Northern Hemisphere, but $PM_{2.5}$ levels increased over the Southern Hemisphere and oceans. These findings are consistent with those of (Murray et al., 2024), who highlighted how increased precipitation enhances $PM_{2.5}$ removal via wet deposition. We newly found that increased wind speeds also contribute significantly to $PM_{2.5}$ reduction by promoting pollutant dispersion, particularly in mid-to high-latitude locations.

The most pronounced $PM_{2.5}$ reductions observed were in North America, Europe, and China, where enhanced precipitation and wind speeds contributed to efficient pollutant removal. These patterns are broadly in agreement with those of previous CCM studies (e.g., Westervelt et al., 2016). Notably, although the cited authors reported relatively weak $PM_{2.5}$ sensitivities to the cloud fraction and RH under the CM3 model, we found substantial and spatially coherent influences of both variables globally. This implies that GEOS-Chem driven by GCAP2.0 (as in the present study) better reveals the aerosol-cloud and humidity interactions and therefore captures the roles played by these variables in terms of modulating secondary aerosol formation and wet scavenging.

We conclude that, unlike fully coupled models that include the evolution of emissions and chemical feedback, the use of a CTM with a finer spatial resolution ensures a more straightforward representation of how climate sensitivity affects air quality. This is supported by the broad spatial coverage of statistically significant grid cells in our regression analysis, indicating that the model better captured the localized responses of $PM_{2.5}$ to meteorological drivers.

4.1.2. O_3 projections

Globally, surface O_3 concentrations over both land and oceans decreased across the SSP–RCP scenarios (Fig. 2). The most pronounced reductions were in regions exhibiting limited emissions of O_3 precursors, such as remote marine environments, where warming-induced increases in water vapor levels likely accelerated O_3 removal via chemical and radiative mechanisms. This behavior is consistent with that reported by Murray et al. (2024), who identified similar marine O_3 responses linked to humidity increases that were governed by the Clausius-Clapeyron relationship. Moreover, our spatial patterns align with those of Zanis et al. (2022), who used CMIP6 CCMs to identify strong O_3 sensitivity to temperature over land, and weaker or negative responses over oceans. Although Murray et al. (2024) attributed the marine O_3 reductions in part to the reactive halogen chemistry explicitly represented in their CTM, our GEOS-Chem does not include the interactive bromine chemistry of sea salt. Thus, our O_3 reductions over oceans are attributable solely to climate-driven meteorological processes such as increased water vapor levels and temperature. Our findings highlight the important roles of fundamental climate processes-including temperature, cloud fraction, and relative humidity-in modulating O_3 concentrations (Table 4), while emphasizing that the response to each variable reflects their combined and interrelated influences rather than independent effects.

4.2. Health implications of future air-quality changes

We compared the health mortality assessment of our study to that of West et al. (2013). We found that, whereas the cited authors projected substantial health co-benefits from simultaneous greenhouse gas mitigation and emission reductions, our fixed-emissions approach revealed that climate-driven meteorological changes alone can also yield meaningful decreases in $PM_{2.5}$- and O_3-related premature mortality. Although the numbers of deaths avoided in our study are smaller than those of the cited authors because we did not consider emission controls, our results demonstrate that climate changes independently influence air-quality and health outcomes.

Furthermore, compared to the BaU scenario that assumes evolving anthropogenic emissions without accounting for climate effects, our climate-driven simulations reveal pollutant-specific health outcomes. $PM_{2.5}$-related mortality under BaU increases through mid-century and declines by the end of the century, reflecting the projected emission reductions. In contrast, our simulations show a more modest decline in $PM_{2.5}$ mortality at mid-century, and even elevated mortality by the end of the century, because of climate-induced increases in pollutant concentrations.

Moreover, even identical pollutant concentrations may yield different health outcomes under intensified climate stress–such as higher temperatures and humidity extremes–expected in high-forcing scenarios like SSP5-8.5. This underscores that our mortality estimates represent concentration-driven responses only, without accounting for the potential amplification of health risks under severe future climate conditions. In contrast, O_3-related mortality consistently decreases in our climate-driven projections, implying that meteorological changes alone can yield substantial health co-benefits, even in the absence of direct emission controls. This difference may, at least in part, reflect methane emission increases under the SSP2-based BaU scenario, which can enhance background O_3 concentrations and contribute to higher ozone-related mortality relative to the climate-driven simulations.

4.3. Limitations

Our study had certain limitations that we will address in future. First, our study employs GEOS-Chem in a one-way coupled to GCAP2.0 configuration. As a result, the model does not represent aerosol–radiation or aerosol–cloud interactions and therefore cannot explicitly capture the bidirectional feedback between air pollutants and meteorology. However, because our objective was to isolate the sensitivity of $PM_{2.5}$ and O_3 concentrations to meteorology-only changes under constant emissions, the one-way framework provides a transparent and interpretable setup in which concentration differences can be attributed solely to prescribed meteorological changes. Consequently, the absence of two-way coupling does not bias our results in the sense of producing incorrect future projections, as we do not attempt to simulate the fully coupled atmosphere–chemistry system associated with evolving SSP–RCP emissions. However, the magnitude of climate-driven concentration changes may differ in fully coupled Earth system models, and this should be considered when interpreting the results. Although GCAP2.0 meteorology reproduces the large-scale spatial patterns of temperature and precipitation when compared with MERRA-2, residual regional biases–particularly in high-latitude temperature and tropical precipitation–remain inherent to GCM-derived meteorological fields. These uncertainties may influence the magnitude of the simulated $PM_{2.5}$ and O_3 sensitivities and should be considered when interpreting the results. Similarly, the associated mortality estimates represent meteorology-induced exposure sensitivities rather than predictions of future health outcomes under co-evolving climate and emission trajectories.

Second, we did not investigate changes in climate-driven emissions such as wildfires, dust, and biogenic sources, which are projected to intensify strongly under warming and could substantially affect both the $PM_{2.5}$- and O_3-concentration-associated health outcomes (Lee and Jaffe, 2024; Park et al., 2024a, 2024b). We isolated the effects of meteorological conditions to avoid the uncertainties associated with projection of climate-sensitive emissions. However, this exclusion likely means that our estimated climate impacts are conservative lower bounds. Wildfires, dust transport, and biogenic VOCs generally increase pollutant burdens. However, local conditions may yield mixed or indeed offsetting effects, implying that our qualitative conclusions remain robust. Future work should consider climate-sensitive natural emissions for more comprehensive assessment of both air quality and health impacts.

Third, we did not consider the interannual variations in–and climate extremes of–meteorological conditions that would influence $PM_{2.5}$ and O_3 concentrations. Our purpose was to evaluate how long-term weather pattern changes will affect global air quality by mid-century (2040–2049) and the end of the century (2090–2099). This minimized the effects of interannual short-term meteorological fluctuations and emphasized the climate-induced long-term trends. However, future studies should consider the effects of interannual variations and climate extremes (in terms of meteorological conditions) on air quality. This would yield insights into short-term fluctuations and their implications in terms of regional air-quality management.

Finally, this study derived health-impact assessments for $PM_{2.5}$- and O_3-related mortality under the assumption that all future scenarios exhibited the same population exposure. This isolated the impacts of global air quality induced solely by meteorological conditions and climate change under different SSP–RCP scenarios. We did not consider population aging or the fact that mortality increases with age. These assumptions are significant (Turnock et al., 2023; H. Yang et al., 2023). Future studies should consider changes in population size, age structure, and baseline mortality to ensure a comprehensive understanding of future air-pollution-related mortality. This would aid public-health planning/policymaking under different climate scenarios.

5. Conclusion

This study assessed the long-term impacts of climate-driven meteorological changes on global air quality and health. We used the GEOS-Chem model driven by GCAP2.0 meteorological data under multiple climate scenarios. To provide a global perspective on how meteorological conditions and climate change affect $PM_{2.5}$ and O_3 levels, we assessed future global air quality under three SSP–RCP scenarios (SSP1–2.6, SSP2–4.5 and SSP5–8.5).

It is essential to consider meteorological and climate impacts on global air quality. Although emissions remain the primary driver of pollution, meteorological variations including temperature, humidity, wind patterns, and other variables influence pollutant distribution, chemical transformation, and removal. Meteorological changes mitigated air-pollutant levels under SSP1–2.6. The moderate weather conditions of SSP2–4.5 either decreased or increased air-pollutant concentrations. Although SSP5–8.5 is characterized by an extreme climate, air quality did not uniformly worsen. Enhanced atmospheric dispersion and scavenging in certain areas removed some pollutants. We conclude that regional and seasonal meteorological changes impact air pollutant concentrations.

Despite the relatively small changes in global $PM_{2.5}$ and O_3 concentrations, the health impacts were non-negligible, resulting in substantial numbers of avoided deaths across all SSP–RCP scenarios. By quantifying the impact of climate change on air pollutants and associated health outcomes, our results confirm the initial hypothesis: climate-driven meteorological conditions greatly affect future global air quality and health and must therefore be explicitly incorporated into global air-quality assessments to ensure robust evaluation of future risks.

CRediT authorship contribution statement

Racha Samermit: Writing – review & editing, Writing – original draft, Visualization, Validation, Methodology, Formal analysis, Conceptualization. **Thanapat Jansakoo:** Writing – review & editing, Conceptualization. **Shinichiro Fujimori:** Writing – review & editing, Supervision, Conceptualization. **Saritha Sudharmma Vishwanathan:** Writing – review & editing.

Code availability

GEOS-Chem (GCClassic) version 14.1.1 code is available at https://github.com/geoschem/geos-chem. All codes used for visualization of the figures are available at https://github.com/Racha711/Analysis_RS.git.

Declaration of generative AI and AI-assisted technologies in the writing process

The authors declare that no generative AI or AI-assisted technologies were employed for conceptual or substantive content generation, data analysis, or decision-making processes related to the manuscript.

Declaration of competing interest

The authors declare that they have no known competing financial interests or personal relationships that could have appeared to influence the work reported in this paper.

Acknowledgements

This study was partially funded by the Environment Research and Technology Development Fund (JPMEERF20241001) of the Environmental Restoration and Conservation Agency of Japan, supported by the Ministry of the Environment, Japan, and by the Sumitomo Electric Industries Group CSR Foundation (Japan). This work was also supported by the Japan Science and Technology Agency (JST) under the Adopting Sustainable Partnerships for Innovative Research Ecosystem (ASPIRE) program (JPMJAP2331). Part of this research was conducted using a supercomputer at the Academic Center for Computing and Media Studies, Kyoto University, Japan.

Appendix A. Supplementary data

Supplementary data to this article can be found online at https://doi.org/10.1016/j.aeaoa.2026.100430.

Data availability

The datasets of GCAP2.0 meteorological fields and CMIP6 anthropogenic emission and boundary conditions can be accessed via http://atmos.earth.rochester.edu/input/gc/ExtData.

References

Andersson, C., Langner, J., 2007. Inter-annual variations of ozone and nitrogen dioxide over Europe during 1958–2003 simulated with a regional CTM. Water air soil pollut. Focus 7, 15–23. https://doi.org/10.1007/s11267-006-9088-4.

Bey, I., Jacob, D.J., Yantosca, R.M., Logan, J.A., Field, B.D., Fiore, A.M., Li, Q., Liu, H.Y., Mickley, L.J., Schultz, M.G., 2001. Global modeling of tropospheric chemistry with assimilated meteorology: model description and evaluation. J. Geophys. Res. Atmospheres 106, 23073–23095. https://doi.org/10.1029/2001jd000807.

Burnett, R.T., Pope, C.A., Ezzati, M., Olives, C., Lim, S.S., Mehta, S., Shin, H.H., Singh, G., Hubbell, B., Brauer, M., Anderson, H.R., Smith, K.R., Balmes, J.R., Bruce, N.G., Kan, H., Laden, F., Prüss-Ustün, A., Turner, M.C., Gapstur, S.M., Diver, W.R., Cohen, A., 2014. An integrated risk function for estimating the global burden of disease attributable to ambient fine particulate matter exposure. Environ. Health Perspect. 122, 397–403. https://doi.org/10.1289/ehp.1307049.

Dang, R., Liao, H., Fu, Y., 2021. Quantifying the anthropogenic and meteorological influences on summertime surface ozone in China over 2012–2017. Sci. Total Environ. 754, 142394. https://doi.org/10.1016/j.scitotenv.2020.142394.

Dawson, J.P., Adams, P.J., Pandis, S.N., 2007. Sensitivity of PM2.5 to climate in the Eastern US: a modeling case study. Atmos. Chem. Phys. 7, 4295–4309. https://doi.org/10.5194/acp-7-4295-2007.

Dimakopoulou, K., Douros, J., Samoli, E., Karakatsani, A., Rodopoulou, S., Papakosta, D., Grivas, G., Tsilingiridis, G., Mudway, I., Moussiopoulos, N., Katsouyanni, K., 2020. Long-term exposure to ozone and children's respiratory health: results from the RESPOZE study. Environ. Res. 182, 109002. https://doi.org/10.1016/j.envres.2019.109002.

Doherty, R.M., Wild, O., Shindell, D.T., Zeng, G., MacKenzie, I.A., Collins, W.J., Fiore, A.M., Stevenson, D.S., Dentener, F.J., Schultz, M.G., Hess, P., Derwent, R.G., Keating, T.J., 2013. Impacts of climate change on surface ozone and intercontinental ozone pollution: a multi-model study. J. Geophys. Res. Atmospheres 118, 3744–3763. https://doi.org/10.1002/jgrd.50266.

EPA, 2013. Integrated Science Assessment for Particulate Matter (No. EPA/600/R–12/056F). United States Environmental Protection Agency (EPA), Washington, DC.

Fang, Y., Mauzerall, D.L., Liu, J., Fiore, A.M., Horowitz, L.W., 2013. Impacts of 21st century climate change on global air pollution-related premature mortality. Clim. Change 121, 239–253. https://doi.org/10.1007/s10584-013-0847-8.

Feng, J.L., Guo, Z.G., Zhang, T.R., Yao, X.H., Chan, C.K., Fang, M., 2012. Source and formation of secondary particulate matter in $PM_{2.5}$ in Asian continental outflow. J. Geophys. Res. Atmospheres 117. https://doi.org/10.1029/2011JD016400, 2011JD016400.

Fiore, A.M., Naik, V., Spracklen, D.V., Steiner, A., Unger, N., Prather, M., Bergmann, D., Cameron-Smith, P.J., Cionni, I., Collins, W.J., Dalsøren, S., Eyring, V., Folberth, G.A., Ginoux, P., Horowitz, L.W., Josse, B., Lamarque, J.-F., MacKenzie, I.A., Nagashima, T., O'Connor, F.M., Righi, M., Rumbold, S.T., Shindell, D.T., Skeie, R.B., Sudo, K., Szopa, S., Takemura, T., Zeng, G., 2012. Global air quality and climate. Chem. Soc. Rev. 41, 6663. https://doi.org/10.1039/c2cs35095e.

Fujimori, S., Abe, M., Kinoshita, T., Hasegawa, T., Kawase, H., Kushida, K., Masui, T., Oka, K., Shiogama, H., Takahashi, K., Tatebe, H., Yoshikawa, M., 2017. Downscaling global emissions and its implications derived from climate model experiments. PLoS One 12, e0169733. https://doi.org/10.1371/journal.pone.0169733.

Fujimori, S., Hasegawa, T., Ito, A., Takahashi, K., Masui, T., 2018. Gridded emissions and land-use data for 2005–2100 under diverse socioeconomic and climate mitigation scenarios. Sci. Data 5, 180210. https://doi.org/10.1038/sdata.2018.210.

Gidden, M.J., Riahi, K., Smith, S.J., Fujimori, S., Luderer, G., Kriegler, E., Van Vuuren, D.P., Van Den Berg, M., Feng, L., Klein, D., Calvin, K., Doelman, J.C., Frank, S., Fricko, O., Harmsen, M., Hasegawa, T., Havlik, P., Hilaire, J., Hoesly, R., Horing, J., Popp, A., Stehfest, E., Takahashi, K., 2019. Global emissions pathways under different socioeconomic scenarios for use in CMIP6: a dataset of harmonized emissions trajectories through the end of the century. Geosci. Model Dev. 12, 1443–1475. https://doi.org/10.5194/gmd-12-1443-2019.

Gong, S.L., 2003. A parameterization of sea-salt aerosol source function for sub- and super-micron particles. Glob. Biogeochem. Cycles 17. https://doi.org/10.1029/2003gb002079.

Guenther, A.B., Jiang, X., Heald, C.L., Sakulyanontvittaya, T., Duhl, T., Emmons, L.K., Wang, X., 2012. The Model of Emissions of Gases and Aerosols from Nature version 2.1 (MEGAN2.1): an extended and updated framework for modeling biogenic emissions. Geosci. Model Dev. 5, 1471–1492. https://doi.org/10.5194/gmd-5-1471-2012.

Hoesly, R.M., Smith, S.J., Feng, L., Klimont, Z., Janssens-Maenhout, G., Pitkanen, T., Seibert, J.J., Vu, L., Andres, R.J., Bolt, R.M., Bond, T.C., Dawidowski, L., Kholod, N., Kurokawa, J., Li, M., Liu, L., Lu, Z., Moura, M.C.P., O'Rourke, P.R., Zhang, Q., 2018. Historical (1750–2014) anthropogenic emissions of reactive gases and aerosols from the Community Emissions Data System (CEDS). Geosci. Model Dev. 11, 369–408. https://doi.org/10.5194/gmd-11-369-2018.

Hu, L., Keller, C.A., Long, M.S., Sherwen, T., Auer, B., Da Silva, A., Nielsen, J.E., Pawson, S., Thompson, M.A., Trayanov, A.L., Travis, K.R., Grange, S.K., Evans, M.J., Jacob, D.J., 2018. Global simulation of tropospheric chemistry at 12.5 km resolution: performance and evaluation of the GEOS-Chem chemical module (v10-1) within the NASA GEOS Earth system model (GEOS-5 ESM). Geosci. Model Dev. 11, 4603–4620. https://doi.org/10.5194/gmd-11-4603-2018.

Hua, Y., Wang, S., Wang, J., Jiang, J., Zhang, T., Song, Y., Kang, L., Zhou, W., Cai, R., Wu, D., Fan, S., Wang, T., Tang, X., Wei, Q., Sun, F., Xiao, Z., 2016. Investigating the impact of regional transport on $PM_{2.5}$ formation using vertical observation during APEC 2014 Summit in Beijing. Atmos. Chem. Phys. 16, 15451–15460. https://doi.org/10.5194/acp-16-15451-2016.

Hudman, R.C., Moore, N.E., Mebust, A.K., Martin, R.V., Russell, A.R., Valin, L.C., Cohen, R.C., 2012. Steps towards a mechanistic model of global soil nitric oxide emissions: implementation and space based-constraints. Atmos. Chem. Phys. 12, 7779–7795. https://doi.org/10.5194/acp-12-7779-2012.

Im, U., Bauer, S.E., Frohn, L.M., Geels, C., Tsigaridis, K., Brandt, J., 2023. Present-day and future PM2.5 and O3-related global and regional premature mortality in the EVAv6.0 health impact assessment model. Environ. Res. 216, 114702. https://doi.org/10.1016/j.envres.2022.114702.

IPCC, 2023. Climate Change 2023: Synthesis Report. Contribution of Working Groups I, II and III to the Sixth Assessment Report of the Intergovernmental Panel on Climate Change. IPCC, Geneva, Switzerland. https://doi.org/10.59327/IPCC/AR6-9789291691647.

Jacob, D.J., Winner, D.A., 2009. Effect of climate change on air quality. Atmos. Environ., Atmospheric Environment - Fifty Years of Endeavour 43, 51–63. https://doi.org/10.1016/j.atmosenv.2008.09.051.

Jansakoo, T., Sekizawa, S., Fujimori, S., Hasegawa, T., Oshiro, K., 2024a. Benefits of air quality for human health resulting from climate change mitigation through dietary change and food loss prevention policy. Sustain. Sci. 19, 1391–1407. https://doi.org/10.1007/s11625-024-01490-w.

Jansakoo, T., Watanabe, R., Uetani, A., Sekizawa, S., Fujimori, S., Hasegawa, T., Oshiro, K., 2024b. Comparison of global air pollution impacts across horizontal resolutions. Atmos. Environ. X 24, 100303. https://doi.org/10.1016/j.aeaoa.2024.100303.

Jerrett, M., Burnett, R.T., Pope, C.A., Ito, K., Thurston, G., Krewski, D., Shi, Y., Calle, E., Thun, M., 2009. Long-term ozone exposure and mortality. N. Engl. J. Med. 360, 1085–1095. https://doi.org/10.1056/NEJMoa0803894.

Jones, B., O'Neill, B.C., 2016. Spatially explicit global population scenarios consistent with the shared socioeconomic pathways. Environ. Res. Lett. 11, 084003. https://doi.org/10.1088/1748-9326/11/8/084003.

Keller, C.A., Long, M.S., Yantosca, R.M., Da Silva, A.M., Pawson, S., Jacob, D.J., 2014. HEMCO v1.0: a versatile, ESMF-compliant component for calculating emissions in atmospheric models. Geosci. Model Dev. 7, 1409–1417. https://doi.org/10.5194/gmd-7-1409-2014.

Kelley, M., Schmidt, G.A., Nazarenko, L.S., Bauer, S.E., Ruedy, R., Russell, G.L., Ackerman, A.S., Aleinov, I., Bauer, M., Bleck, R., Canuto, V., Cesana, G., Cheng, Y., Clune, T.L., Cook, B.I., Cruz, C.A., Del Genio, A.D., Elsaesser, G.S., Faluvegi, G., Kiang, N.Y., Kim, D., Lacis, A.A., Leboissetier, A., LeGrande, A.N., Lo, K.K., Marshall, J., Matthews, E.E., McDermid, S., Mezuman, K., Miller, R.L., Murray, L.T., Oinas, V., Orbe, C., García-Pando, C.P., Perlwitz, J.P., Puma, M.J., Rind, D., Romanou, A., Shindell, D.T., Sun, S., Tausnev, N., Tsigaridis, K., Tselioudis, G., Weng, E., Wu, J., Yao, M., 2020. GISS-E2.1: configurations and climatology. J. Adv. Model. Earth Syst. 12. https://doi.org/10.1029/2019ms002025.

Kinney, P.L., 2008. Climate change, air quality, and human health. Am. J. Prev. Med. 35, 459–467. https://doi.org/10.1016/j.amepre.2008.08.025.

Koo, B., Jung, J., Pollack, A.K., Lindhjem, C., Jimenez, M., Yarwood, G., 2012. Impact of meteorology and anthropogenic emissions on the local and regional ozone weekend effect in Midwestern US. Atmos. Environ. 57, 13–21. https://doi.org/10.1016/j.atmosenv.2012.04.043.

Krishnaveni, A.S., Madhavan, B.L., Jain, C.D., Venkat Ratnam, M., 2024. Spatial, temporal features and influence of meteorology on PM2.5 and O3 association across urban and rural environments of India. Atmos. Environ. X 22, 100265. https://doi.org/10.1016/j.aeaoa.2024.100265.

Lam, Y.F., Fu, J.S., Wu, S., Mickley, L.J., 2011. Impacts of future climate change and effects of biogenic emissions on surface ozone and particulate matter concentrations in the United States. Atmos. Chem. Phys. 11, 4789–4806. https://doi.org/10.5194/acp-11-4789-2011.

Lee, H., Jaffe, D.A., 2024. Wildfire impacts on O_3 in the Continental United States using $PM_{2.5}$ and a generalized additive model (2018–2023). Environ. Sci. Technol. 58, 14764–14774. https://doi.org/10.1021/acs.est.4c05870.

Lin, H., Ding, K., Huang, X., Lou, S., Xue, L., Wang, Z., Ma, Y., Ding, A., 2024. Impacts of Northward typhoons on autumn haze pollution over North China Plain. J. Geophys. Res. Atmospheres 129, e2023JD040465. https://doi.org/10.1029/2023JD040465.

Lou, S., Liao, H., Yang, Y., Mu, Q., 2015. Simulation of the interannual variations of tropospheric ozone over China: roles of variations in meteorological parameters and anthropogenic emissions. Atmos. Environ. 122, 839–851. https://doi.org/10.1016/j.atmosenv.2015.08.081.

Malashock, D.A., Delang, M.N., Becker, J.S., Serre, M.L., West, J.J., Chang, K.-L., Cooper, O.R., Anenberg, S.C., 2022. Global trends in ozone concentration and attributable mortality for urban, peri-urban, and rural areas between 2000 and 2019: a modelling study. Lancet Planet. Health 6, e958–e967. https://doi.org/10.1016/s2542-5196(22)00260-1.

Mao, J., Paulot, F., Jacob, D.J., Cohen, R.C., Crounse, J.D., Wennberg, P.O., Keller, C.A., Hudman, R.C., Barkley, M.P., Horowitz, L.W., 2013. Ozone and organic nitrates over the eastern United States: sensitivity to isoprene chemistry. J. Geophys. Res. Atmospheres 118. https://doi.org/10.1002/jgrd.50817.

Miller, K.A., Siscovick, D.S., Sheppard, L., Shepherd, K., Sullivan, J.H., Anderson, G.L., Kaufman, J.D., 2007. Long-term exposure to air pollution and incidence of cardiovascular events in women. N. Engl. J. Med. 356, 447–458. https://doi.org/10.1056/NEJMoa054409.

Murray, L.T., Leibensperger, E.M., Mickley, L.J., Tai, A.P.K., 2024. Estimating future climate change impacts on human mortality and crop yields via air pollution. Proc. Natl. Acad. Sci. 121. https://doi.org/10.1073/pnas.2400117121.

Murray, L.T., Leibensperger, E.M., Orbe, C., Mickley, L.J., Sulprizio, M., 2021. Gcap 2.0: a global 3-D chemical-transport model framework for past, present, and future climate scenarios. Geosci. Model Dev. 14, 5789–5823. https://doi.org/10.5194/gmd-14-5789-2021.

Nazarenko, L., Schmidt, G.A., Miller, R.L., Tausnev, N., Kelley, M., Ruedy, R., Russell, G. L., Aleinov, I., Bauer, M., Bauer, S., Bleck, R., Canuto, V., Cheng, Y., Clune, T.L., Del Genio, A.D., Faluvegi, G., Hansen, J.E., Healy, R.J., Kiang, N.Y., Koch, D., Lacis, A.A., LeGrande, A.N., Lerner, J., Lo, K.K., Menon, S., Oinas, V., Perlwitz, J., Puma, M.J., Rind, D., Romanou, A., Sato, M., Shindell, D.T., Sun, S., Tsigaridis, K., Unger, N., Voulgarakis, A., Yao, M.-S., Zhang, J., 2015. Future climate change under RCP emission scenarios with GISS ModelE2. J. Adv. Model. Earth Syst. 7, 244–267. https://doi.org/10.1002/2014ms000403.

Nightingale, P.D., Liss, P.S., Schlosser, P., 2000a. Measurements of air-sea gas transfer during an open ocean algal bloom. Geophys. Res. Lett. 27, 2117–2120. https://doi.org/10.1029/2000gl011541.

Nightingale, P.D., Malin, G., Law, C.S., Watson, A.J., Liss, P.S., Liddicoat, M.I., Boutin, J., Upstill-Goddard, R.C., 2000b. In situ evaluation of air-sea gas exchange parameterizations using novel conservative and volatile tracers. Glob. Biogeochem. Cycles 14, 373–387. https://doi.org/10.1029/1999gb900091.

Nolte, C.G., Spero, T.L., Bowden, J.H., Mallard, M.S., Dolwick, P.D., 2018. The potential effects of climate change on air quality across the conterminous US at 2030 under three representative concentration pathways. Atmos. Chem. Phys. 18, 15471–15489. https://doi.org/10.5194/acp-18-15471-2018.

O'Neill, B.C., Tebaldi, C., Van Vuuren, D.P., Eyring, V., Friedlingstein, P., Hurtt, G., Knutti, R., Kriegler, E., Lamarque, J.-F., Lowe, J., Meehl, G.A., Moss, R., Riahi, K., Sanderson, B.M., 2016. The scenario model intercomparison project (ScenarioMIP) for CMIP6. Geosci. Model Dev. 9, 3461–3482. https://doi.org/10.5194/gmd-9-3461-2016.

Park, C.Y., Takahashi, K., Fujimori, S., Jansakoo, T., Burton, C., Huang, H., Kou-Giesbrecht, S., Reyer, C.P.O., Mengel, M., Burke, E., Li, F., Hantson, S., Takakura, J., Lee, D.K., Hasegawa, T., 2024a. Attributing human mortality from fire PM2.5 to climate change. Nat. Clim. Change 14, 1193–1200. https://doi.org/10.1038/s41558-024-02149-1.

Park, C.Y., Takahashi, K., Fujimori, S., Phung, V.L.H., Li, F., Takakura, J., Hasegawa, T., Jansakoo, T., 2024b. Future fire-$PM_{2.5}$ mortality varies depending on climate and socioeconomic changes. Environ. Res. Lett. 19, 024003. https://doi.org/10.1088/1748-9326/ad1b7d.

Parrella, J.P., Jacob, D.J., Liang, Q., Zhang, Y., Mickley, L.J., Miller, B., Evans, M.J., Yang, X., Pyle, J.A., Theys, N., Van Roozendael, M., 2012. Tropospheric bromine chemistry: implications for present and pre-industrial ozone and mercury. Atmos. Chem. Phys. 12, 6723–6740. https://doi.org/10.5194/acp-12-6723-2012.

Pope, C.A., Dockery, D.W., 2006. Health effects of fine particulate air pollution: lines that connect. J. Air Waste Manag. Assoc. 56, 709–742. https://doi.org/10.1080/10473289.2006.10464485, 1995.

Pope III, C.A., Burnett, R.T., Thun, M.J., Calle, E.E., Krewski, D., Ito, K., Thurston, G.D., 2002. Lung cancer, cardiopulmonary mortality, and long-term exposure to fine particulate air pollution. JAMA 287, 1132–1141. https://doi.org/10.1001/jama.287.9.1132.

Pye, H.O.T., Liao, H., Wu, S., Mickley, L.J., Jacob, D.J., Henze, D.K., Seinfeld, J.H., 2009. Effect of changes in climate and emissions on future sulfate-nitrate-ammonium aerosol levels in the United States. J. Geophys. Res. Atmospheres 114. https://doi.org/10.1029/2008jd010701.

Riahi, K., Van Vuuren, D.P., Kriegler, E., Edmonds, J., O'Neill, B.C., Fujimori, S., Bauer, N., Calvin, K., Dellink, R., Fricko, O., Lutz, W., Popp, A., Cuaresma, J.C., Kc, S., Leimbach, M., Jiang, L., Kram, T., Rao, S., Emmerling, J., Ebi, K., Hasegawa, T., Havlik, P., Humpenöder, F., Da Silva, L.A., Smith, S., Stehfest, E., Bosetti, V., Eom, J., Gernaat, D., Masui, T., Rogelj, J., Strefler, J., Drouet, L., Krey, V., Luderer, G., Harmsen, M., Takahashi, K., Baumstark, L., Doelman, J.C., Kainuma, M., Klimont, Z., Marangoni, G., Lotze-Campen, H., Obersteiner, M., Tabeau, A., Tavoni, M., 2017. The shared socioeconomic pathways and their energy, land use, and greenhouse gas emissions implications: an overview. Glob. Environ. Change 42, 153–168. https://doi.org/10.1016/j.gloenvcha.2016.05.009.

Schnell, J.L., Prather, M.J., Josse, B., Naik, V., Horowitz, L.W., Zeng, G., Shindell, D.T., Faluvegi, G., 2016. Effect of climate change on surface ozone over North America, Europe, and East Asia. Geophys. Res. Lett. 43, 3509–3518. https://doi.org/10.1002/2016gl068060.

Seinfeld, J.H., Pandis, S.N., 2016. Atmospheric Chemistry and Physics from Air Pollution to Climate Change. John Wiley & Sons, Hoboken. - References - Scientific Research Publishing [WWW Document], n.d. URL. https://www.scirp.org/reference/referencespapers?referenceid=2032525, 7.19.25.

Shen, L., Mickley, L.J., Murray, L.T., 2017. Influence of 2000–2050 climate change on particulate matter in the United States: results from a new statistical model. Atmos. Chem. Phys. 17, 4355–4367. https://doi.org/10.5194/acp-17-4355-2017.

Silva, R.A., West, J.J., Lamarque, J.-F., Shindell, D.T., Collins, W.J., Faluvegi, G., Folberth, G.A., Horowitz, L.W., Nagashima, T., Naik, V., Rumbold, S.T., Sudo, K., Takemura, T., Bergmann, D., Cameron-Smith, P., Doherty, R.M., Josse, B., MacKenzie, I.A., Stevenson, D.S., Zeng, G., 2017. Future global mortality from changes in air pollution attributable to climate change. Nat. Clim. Change 7, 647–651. https://doi.org/10.1038/nclimate3354.

Tai, A.P.K., Mickley, L.J., Jacob, D.J., 2012a. Impact of 2000–2050 climate change on fine particulate matter ($PM_{2.5}$) air quality inferred from a multi-model analysis of meteorological modes. Atmos. Chem. Phys. 12, 11329–11337. https://doi.org/10.5194/acp-12-11329-2012.

Tai, A.P.K., Mickley, L.J., Jacob, D.J., 2010. Correlations between fine particulate matter (PM2.5) and meteorological variables in the United States: implications for the sensitivity of PM2.5 to climate change. Atmos. Environ. 44, 3976–3984. https://doi.org/10.1016/j.atmosenv.2010.06.060.

Tai, A.P.K., Mickley, L.J., Jacob, D.J., Leibensperger, E.M., Zhang, L., Fisher, J.A., Pye, H. O.T., 2012b. Meteorological modes of variability for fine particulate matter ($PM_{2.5}$) air quality in the United States: implications for $PM_{2.5}$ sensitivity to climate change. Atmos. Chem. Phys. 12, 3131–3145. https://doi.org/10.5194/acp-12-3131-2012.

Turner, M.C., Jerrett, M., Pope, C.A., Krewski, D., Gapstur, S.M., Diver, W.R., Beckerman, B.S., Marshall, J.D., Su, J., Crouse, D.L., Burnett, R.T., 2016. Long-term ozone exposure and mortality in a large prospective study. Am. J. Respir. Crit. Care Med. 193, 1134–1142. https://doi.org/10.1164/rccm.201508-1633oc.

Turnock, S.T., Allen, R.J., Andrews, M., Bauer, S.E., Deushi, M., Emmons, L., Good, P., Horowitz, L., John, J.G., Michou, M., Nabat, P., Naik, V., Neubauer, D., O'Connor, F. M., Olivié, D., Oshima, N., Schulz, M., Sellar, A., Shim, S., Takemura, T., Tilmes, S., Tsigaridis, K., Wu, T., Zhang, J., 2020. Historical and future changes in air pollutants from CMIP6 models. Atmos. Chem. Phys. 20, 14547–14579. https://doi.org/10.5194/acp-20-14547-2020.

Turnock, S.T., Reddington, C.L., West, J.J., O'Connor, F.M., 2023. The air pollution human health burden in different future scenarios that involve the mitigation of near-term climate forcers, climate and land-use. GeoHealth 7. https://doi.org/10.1029/2023gh000812.

Uchida, H., Yamazaki, K., Sekizawa, S., Fujimori, S., Oshiro, K., Jansakoo, T., 2025. Morbidity changes induced by future air quality and demographic structure changes. Atmos. Environ. X 28, 100396. https://doi.org/10.1016/j.aeaoa.2025.100396.

Von Schneidemesser, E., Monks, P.S., Allan, J.D., Bruhwiler, L., Forster, P., Fowler, D., Lauer, A., Morgan, W.T., Paasonen, P., Righi, M., Sindelarova, K., Sutton, M.A., 2015. Chemistry and the linkages between air quality and climate change. Chem. Rev. 115, 3856–3897. https://doi.org/10.1021/acs.chemrev.5b00089.

Wang, C.-Y., Chen, J.-P., Wang, W.-C., 2023. Meteorology-driven PM2.5 interannual variability over East Asia. Sci. Total Environ. 904, 166911. https://doi.org/10.1016/j.scitotenv.2023.166911.

West, J.J., Smith, S.J., Silva, R.A., Naik, V., Zhang, Y., Adelman, Z., Fry, M.M., Anenberg, S., Horowitz, L.W., Lamarque, J.-F., 2013. Co-benefits of mitigating global greenhouse gas emissions for future air quality and human health. Nat. Clim. Change 3, 885–889. https://doi.org/10.1038/nclimate2009.

Westervelt, D.M., Horowitz, L.W., Naik, V., Tai, A.P.K., Fiore, A.M., Mauzerall, D.L., 2016. Quantifying PM2.5-meteorology sensitivities in a global climate model. Atmos. Environ. 142, 43–56. https://doi.org/10.1016/j.atmosenv.2016.07.040.

WHO, 2021. Ambient (Outdoor) Air Pollution. World Health Organization (WHO), Geneva, Switzerland.

Wu, S., Mickley, L.J., Jacob, D.J., Logan, J.A., Yantosca, R.M., Rind, D., 2007. Why are there large differences between models in global budgets of tropospheric ozone? J. Geophys. Res. Atmospheres 112. https://doi.org/10.1029/2006jd007801.

Wu, S., Mickley, L.J., Jacob, D.J., Rind, D., Streets, D.G., 2008. Effects of 2000–2050 changes in climate and emissions on global tropospheric ozone and the policy-relevant background surface ozone in the United States. J. Geophys. Res. Atmospheres 113. https://doi.org/10.1029/2007jd009639.

Yang, H., Huang, X., Westervelt, D.M., Horowitz, L., Peng, W., 2023a. Socio-demographic factors shaping the future global health burden from air pollution. Nat. Sustain. 6, 58–68. https://doi.org/10.1038/s41893-022-00976-8.

Yang, L., Wang, N., Liu, S., Xiao, Q., Geng, G., Zhang, X., Li, H., Zheng, Y., Guo, F., Li, Q., Li, J., Ren, A., Xue, T., Ji, J., 2023b. The PM2.5 concentration reduction improves survival rate of lung cancer in Beijing. Sci. Total Environ. 858, 159857. https://doi.org/10.1016/j.scitotenv.2022.159857.

Zanis, P., Akritidis, D., Turnock, S., Naik, V., Szopa, S., Georgoulias, A.K., Bauer, S.E., Deushi, M., Horowitz, L.W., Keeble, J., Le Sager, P., O'Connor, F.M., Oshima, N., Tsigaridis, K., Van Noije, T., 2022. Climate change penalty and benefit on surface ozone: a global perspective based on CMIP6 earth system models. Environ. Res. Lett. 17, 024014. https://doi.org/10.1088/1748-9326/ac4a34.

Zender, C.S., Bian, H., Newman, D., 2003. Mineral Dust Entrainment and Deposition (DEAD) model: description and 1990s dust climatology. J. Geophys. Res. Atmospheres 108. https://doi.org/10.1029/2002jd002775.

Zhai, S., Jacob, D.J., Wang, X., Shen, L., Li, K., Zhang, Y., Gui, K., Zhao, T., Liao, H., 2019. Fine particulate matter ($PM_{2.5}$) trends in China, 2013–2018: separating contributions from anthropogenic emissions and meteorology. Atmos. Chem. Phys. 19, 11031–11041. https://doi.org/10.5194/acp-19-11031-2019.